Electronic Supplementary Material (ESI) for Journal of Materials Chemistry C.

MOF sensors for food safety: ultralow detection of putrescine and cadaverine from protein rich foods

T Leelasree,[a] and Himanshu Aggarwal[a*]

[a] Department of Chemistry, Birla Institute of Technology and Science, Hyderabad Campus, Hyderabad 500078, India.

Email: himanshu.aggarwal@hyderabad.bits-pilani.ac.in.

Materials

Cobalt Nitrate hexahydrate [$Co(NO_3)_2.6H_2O$], N,N′- dimethyl formamide were purchased from SRL, biphenyl-4,4'-dicarboxylic acid (bpdc), 1,2-bis(4-pyridyl)ethane (bpe) and 4,4'-bipyridine (bpy) were purchased from TCI chemicals. All the reagents, solvents and analytes Putrescine (PUT), Cadaverine (CAD), Spermine (SPM), Spermidine (SPD), Tyramine (TYRM), Tryptamine (TRYP) were obtained from commercial sources and used as such without additional purification.

Powder X-ray Diffraction (PXRD)

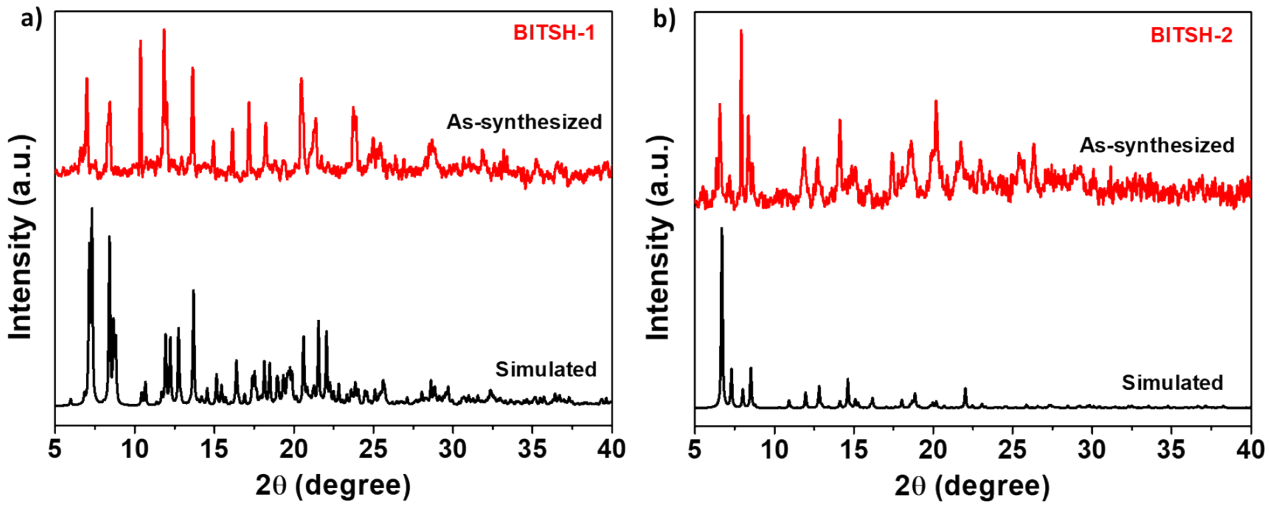

Figure S1. Comparison of the experimental and simulated PXRD patterns of **a)** BITSH-1 and **b)** BITSH-2.

Thermo Gravimetric Analysis (TGA)

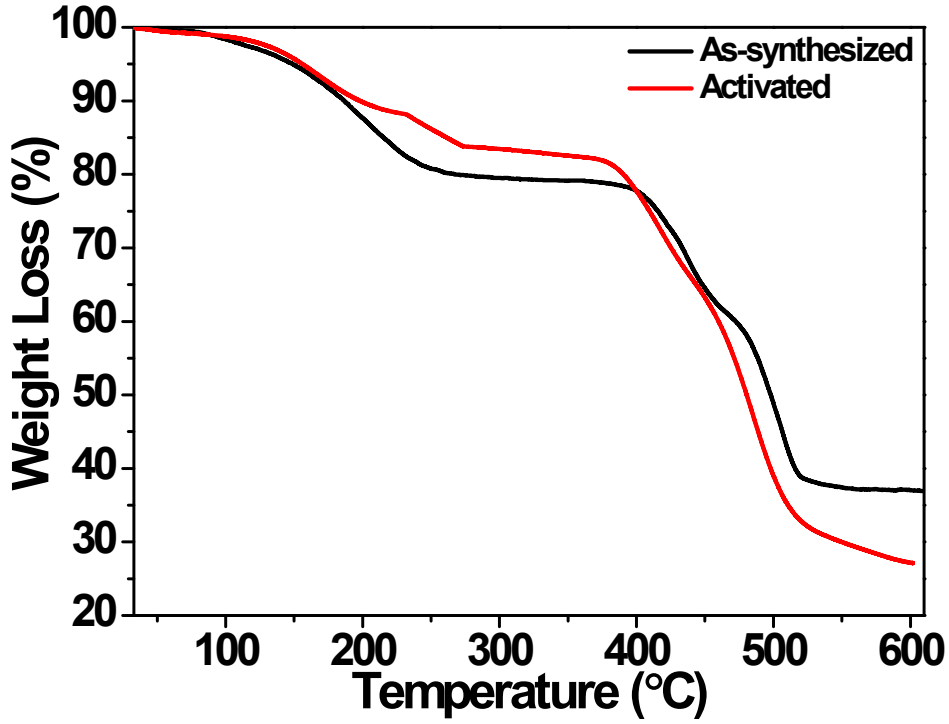

Figure S2. TGA profile of as-synthesized and activated BITSH-1 crystals.

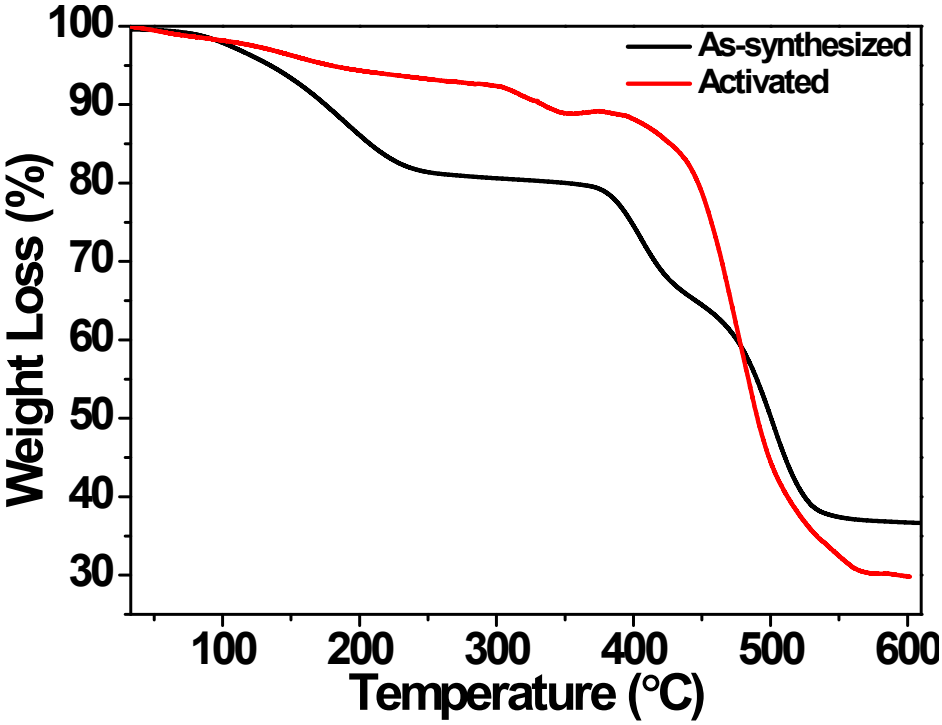

Figure S3. TGA profile of as-synthesized and activated BITSH-2 crystals.

Nitrogen Adsorption Experiments

N_2 adsorption isotherms were performed using Microtrac Bel - BEL SORP mini II model surface area analyzer. The as-synthesized crystals were activated under dynamic vacuum at 90°C for 24hrs before the N_2 sorption measurements. The BET surface area, pore size, and pore volume of both the samples were determined from N_2 sorption isotherms.

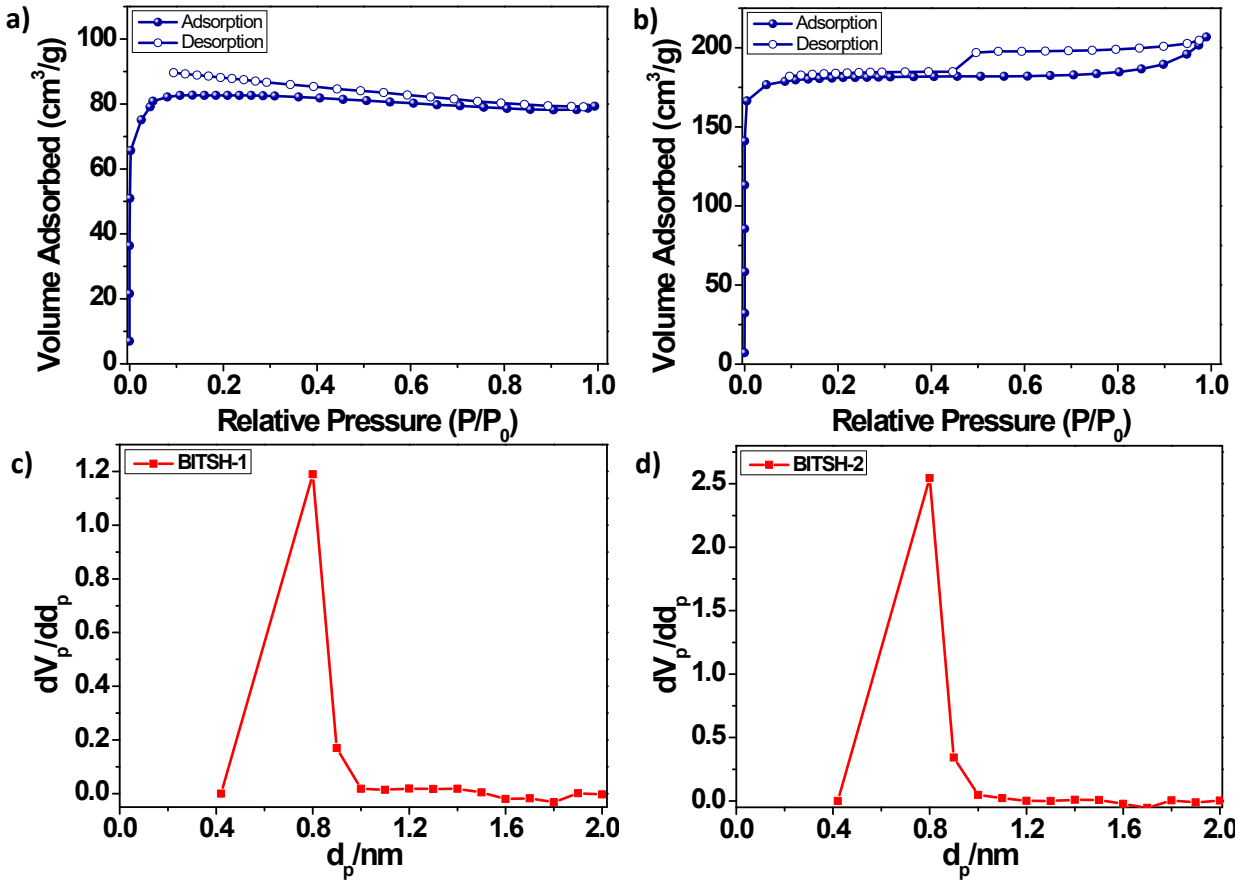

Figure S4. N_2 adsorption isotherm of **a)** BITSH-1 and **b)** BITSH-2 and pore diameter of **c)** BITSH-1 and **d)** BITSH-2 samples.

Field Emission Scanning Electron Microscopy (FE-SEM)

SEM images of both the MOF systems were obtained using FEI Apreo LoVac instrument for surface analysis. The SEM images of the as-synthesized BITSH-1 and BITSH-2 depict block shaped crystals with size ranging from 40 µm – 220 µm.

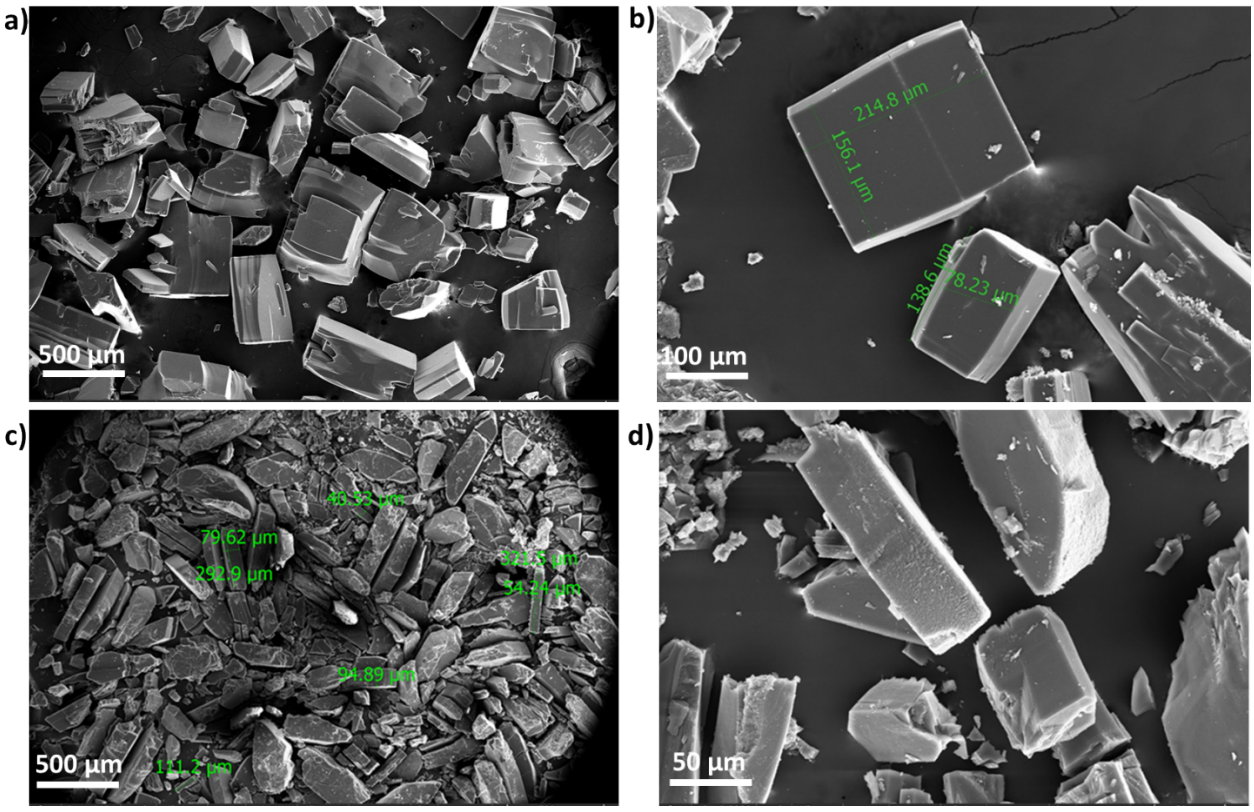

Figure S5. (a) SEM images of BITSH-1 crystals (b) SEM images of BITSH-2 crystals.

Single Crystal X-Ray Diffraction Analysis

The suitable crystals of BITSH-1 and BITSH-2 for single crystal X-ray diffraction (SCXRD) analysis were selected. The SCXRD measurements were performed on the Rigaku XtaLAB P200 diffractometer using graphite monochromated Cu-Kα radiation (λ = 1.54184 Å). The data was collected and reduced using CrysAlisPro (Rigaku Oxford Diffraction) software. The data collection was carried out at 100 K and the structures were solved using Olex2 with the ShelXT structure solution program and refined with the ShelXL refinement package using Least Squares minimization. The details of the crystal data for both compounds is given in Table S1.

The solvent molecules in BITSH-1 could not be modelled with certainty and the structure was squeezed using Olex2 mask function. The structure of BITSH-1 was collected several times and the best possible data set was used for structure elucidation. BITSH-1 contains one molecules of water coordinated to the Co cluster whereas BITSH-2 contains DMF molecules coordinated to the cluster. No disorder was observed for the linker units.

Table S1. Crystallographic data for BITSH-1 and BITSH-2.

Identification code	**BITSH-1**	**BITSH-2**
Empirical formula	$C_{64}H_{62}Co_3N_6O_{17}$	$C_{60}H_{50}Co_3N_4O_{14}$
Formula weight	1363.99	1227.884
Temperature/K	100.0	100
Crystal system	monoclinic	orthorhombic
Space group	$P2_1/n$	*Pbcn*
a/Å	13.8779(3)	13.6216(3)
b/Å	18.0470(4)	26.3669(7)
c/Å	25.8568(5)	20.1175(4)
α/°	90	90
β/°	91.577(2)	90
γ/°	90	90
Volume/Å^3	6473.5(2)	7225.4(3)
Z	4	4
ρ_{calc}g/cm^3	1.400	1.129
μ/mm^{-1}	6.563	5.790
F(000)	2802.9	2505.8
Crystal size/mm^3	0.25 × 0.2 × 0.1	0.1 × 0.05 × 0.02
Radiation	Cu Kα (λ = 1.54184)	Cu Kα (λ = 1.54184)

2Θ range for data collection/°	6.84 to 159.64	8.02 to 160.1
Index ranges	$-17 \leq h \leq 8$, $-22 \leq k \leq 11$, $-32 \leq l \leq 31$	$-8 \leq h \leq 16$, $-32 \leq k \leq 33$, $-25 \leq l \leq 19$
Reflections collected	39926	27877
Independent reflections	13648 [R_{int} = 0.0429, R_{sigma} = 0.0388]	7701 [R_{int} = 0.0507, R_{sigma} = 0.0494]
Data/restraints/parameters	13648/0/815	7701/8/397
Goodness-of-fit on F^2	1.042	1.001
Final R indexes [I>=2σ (I)]	R_1 = 0.0938, wR_2 = 0.2843	R_1 = 0.0617, wR_2 = 0.1756
Final R indexes [all data]	R_1 = 0.1023, wR_2 = 0.2916	R_1 = 0.0749, wR_2 = 0.1867
CCDC	2121260	2121259

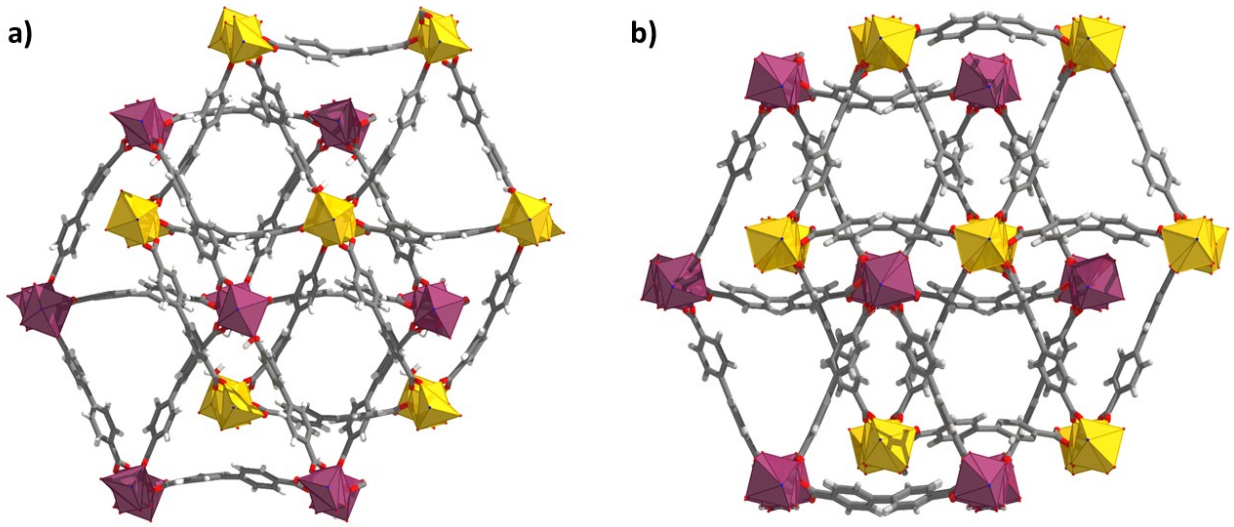

Figure S6. Two-fold interpenetrated structures of a) BITSH-1 and b) BITSH-2. Solvent molecules are omitted for clarity.

Photoluminescence (PL) Measurements

MOF crystals were thoroughly washed with DMF and ethanol. The crystals were vacuum dried and were gently grinded with a mortar pestle. 1 mg of the grinded sample was well dispersed in 2 ml of ethanol via sonication for the measurements. The UV- vis absorbance and PL measurements were carried out for BITSH-1 and BITSH-2. PL studies were carried out with 1 mM concentration of biogenic amines in ethanol medium for both the MOF systems.

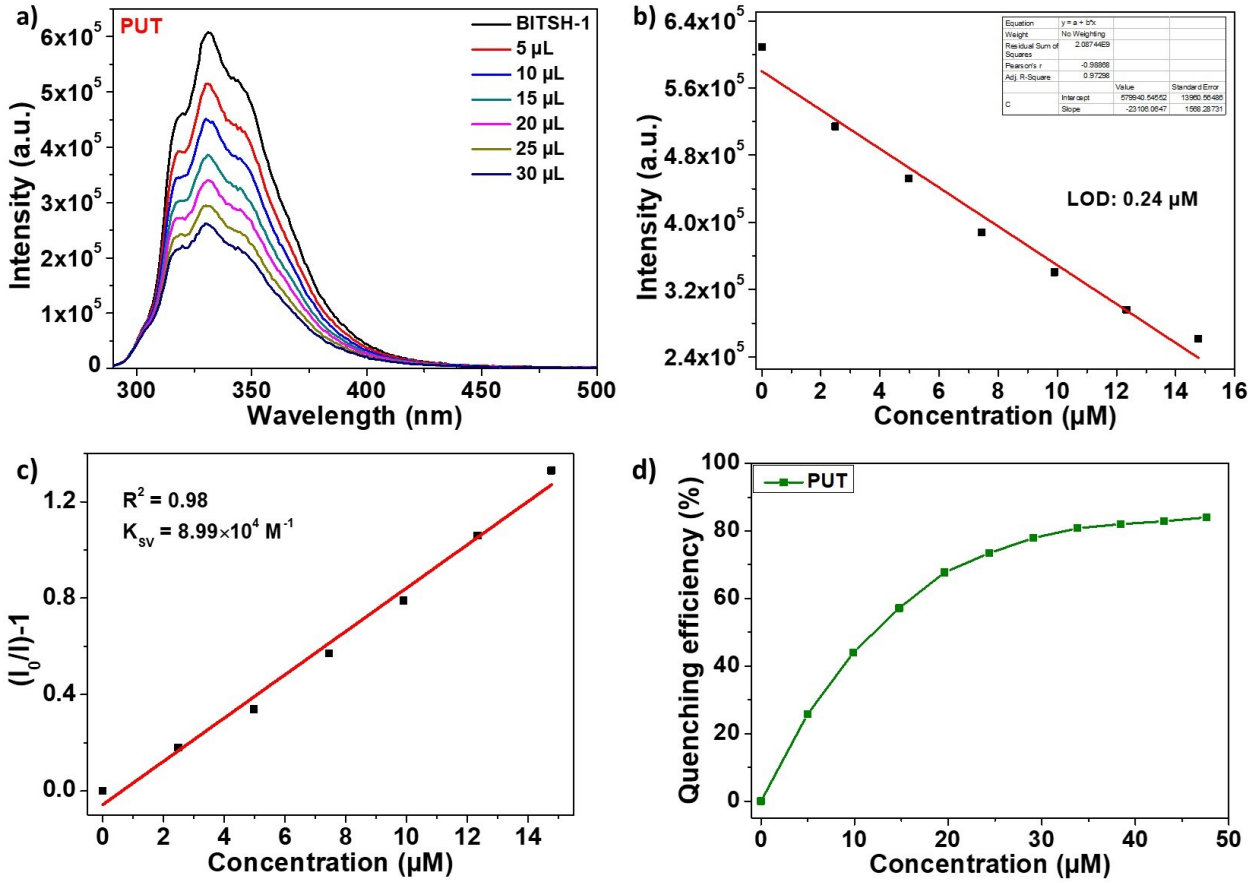

Figure S7. (a) PL emission spectra of BITSH-1 against the incremental additions of 1 mM of putrescine (PUT) in ethanol, (λ_{ex} = 278 nm) **(b)** detection limit (LOD) of PUT, **(c)** linear fit of Stern-Volmer plot of BITSH-1 in response to PUT and **(d)** Quenching efficiency of PUT.

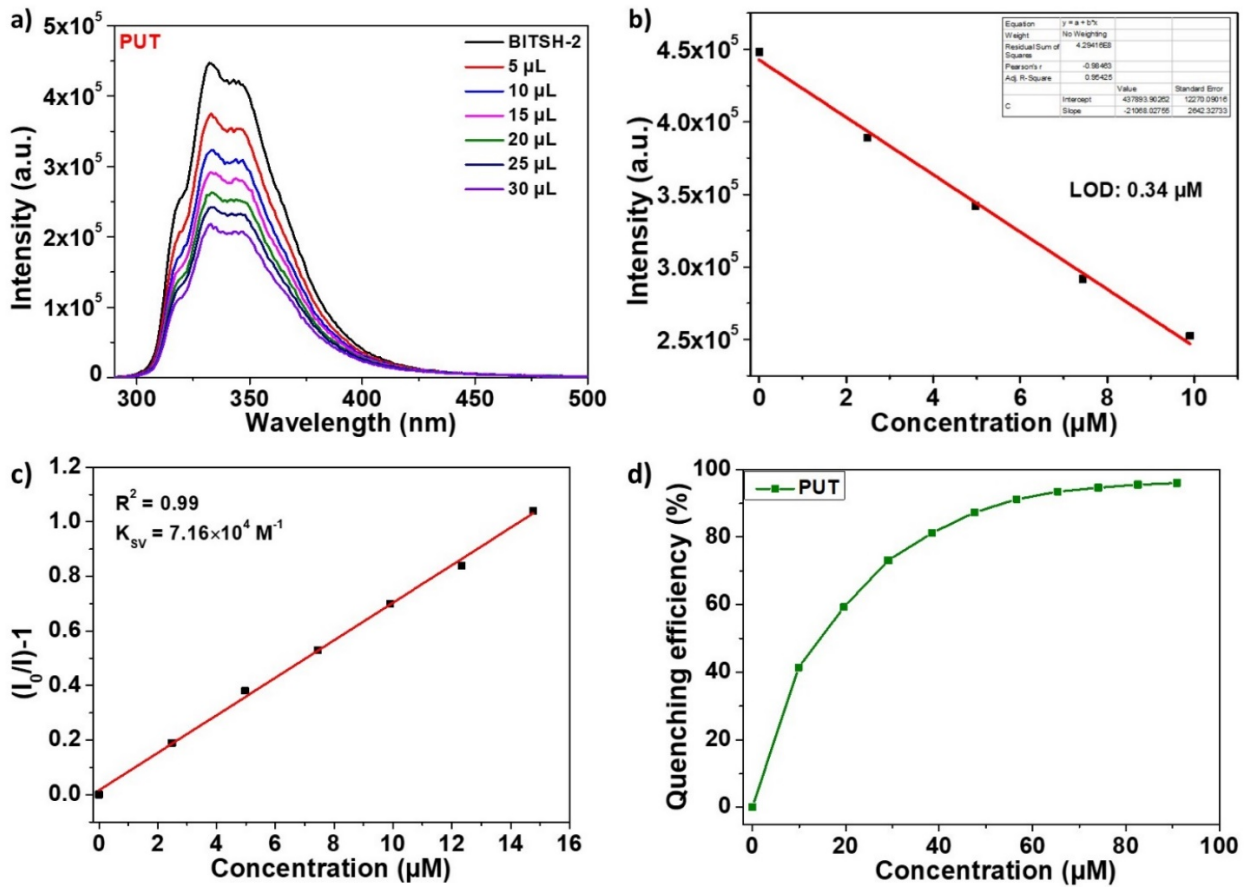

Figure S8. (a) PL emission spectra of BITSH-2 against the incremental additions of 1 mM of putrescine (PUT) in ethanol, (λ_{ex} = 280 nm) **(b)** detection limit (LOD) of PUT, **(c)** linear fit of Stern-Volmer plot of BITSH-2 in response to PUT and **(d)** Quenching efficiency of PUT.

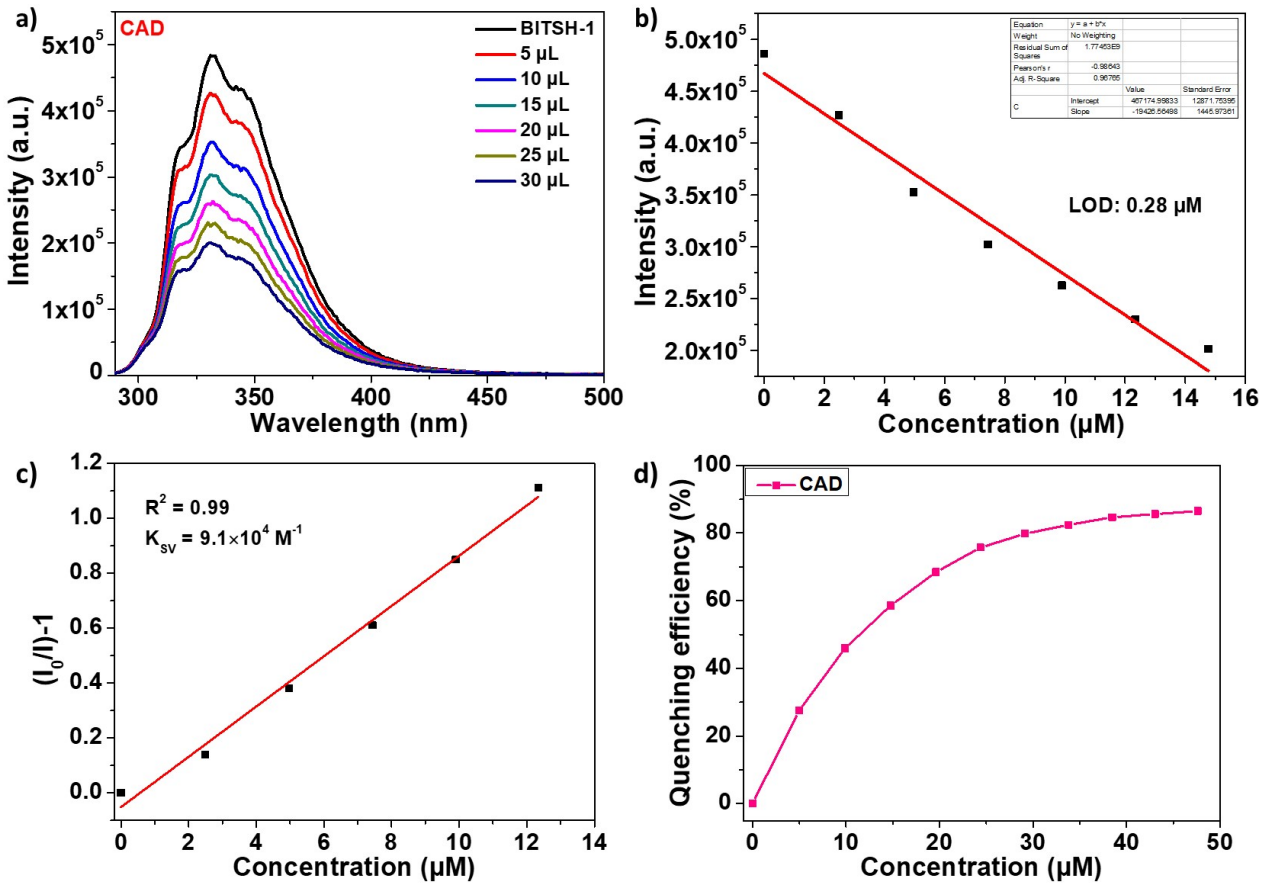

Figure S9. (a) PL emission spectra of BITSH-1 against the incremental additions of 1 mM of cadaverine (CAD) in ethanol, (λ_{ex} = 278 nm) **(b)** detection limit (LOD) of CAD, **(c)** linear fit of Stern-Volmer plot of BITSH-1 in response to CAD and **(d)** Quenching efficiency of CAD.

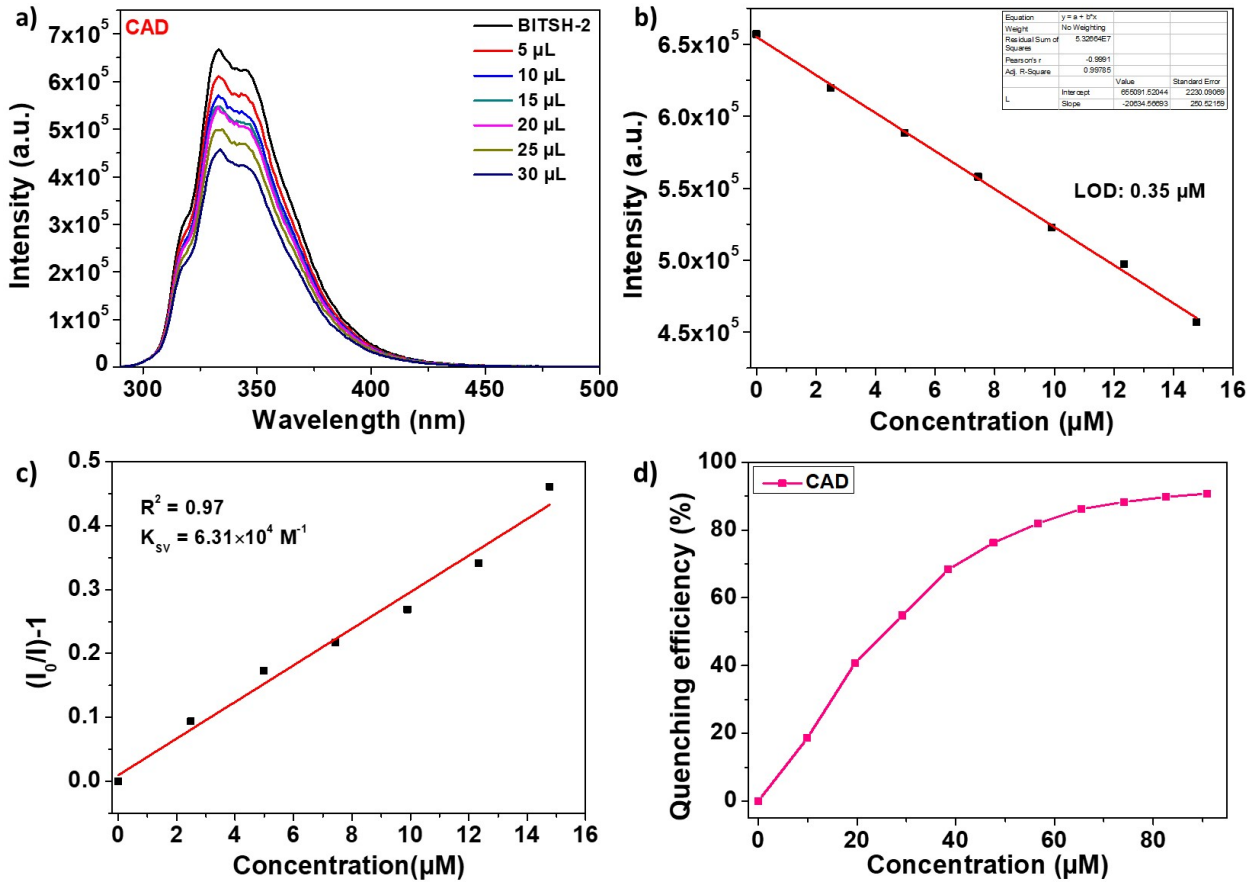

Figure S10. (a) PL emission spectra of BITSH-2 against the incremental additions of 1 mM of cadaverine (CAD) in ethanol, (λ_{ex} = 280 nm) **(b)** detection limit (LOD) of CAD, **(c)** linear fit of Stern-Volmer plot of BITSH-2 in response to CAD and **(d)** Quenching efficiency of CAD.

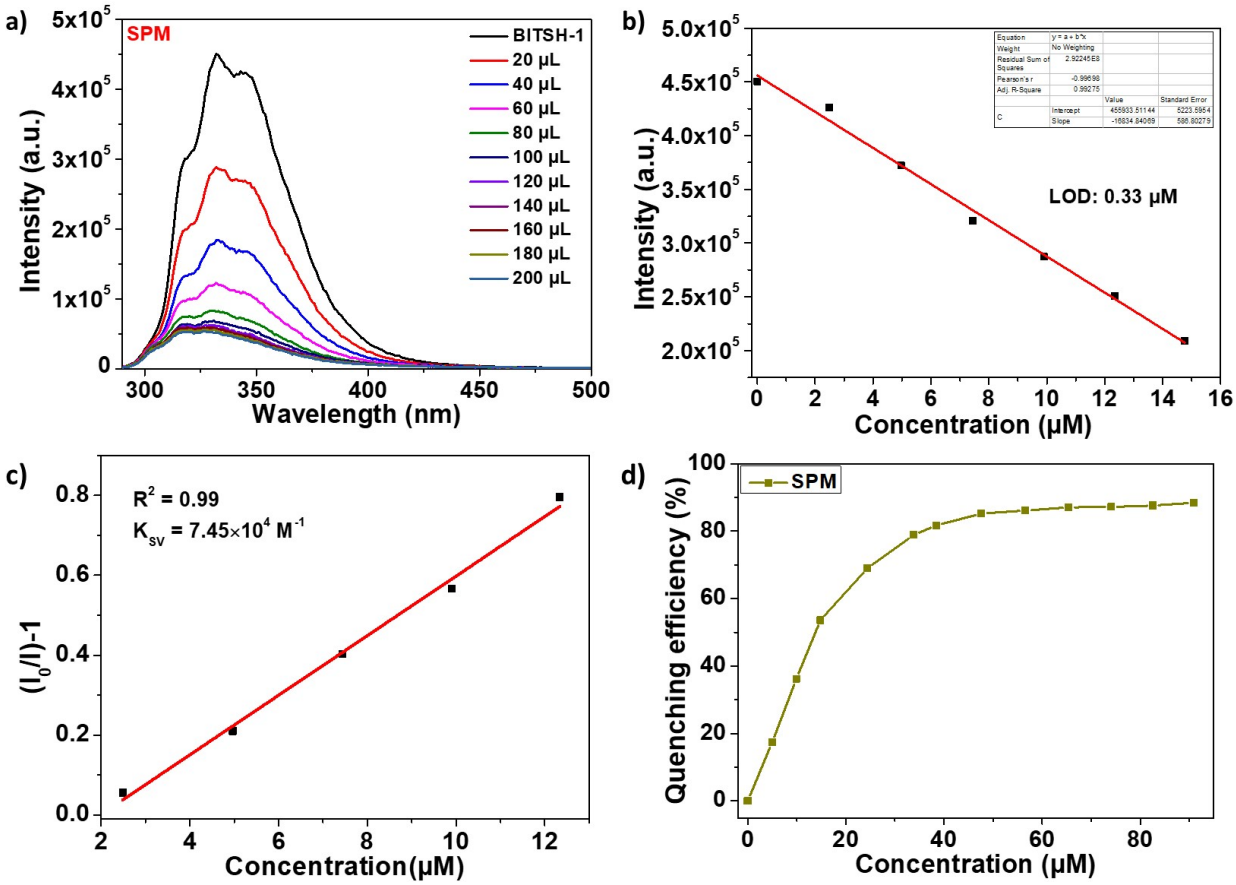

Figure S11. (a) PL emission spectra of BITSH-1 against the incremental additions of 1 mM of spermine (SPM) in ethanol, (λ_{ex} = 278 nm) **(b)** detection limit (LOD) of SPM, **(c)** linear fit of Stern-Volmer plot of BITSH-1 in response to SPM and **(d)** Quenching efficiency of SPM.

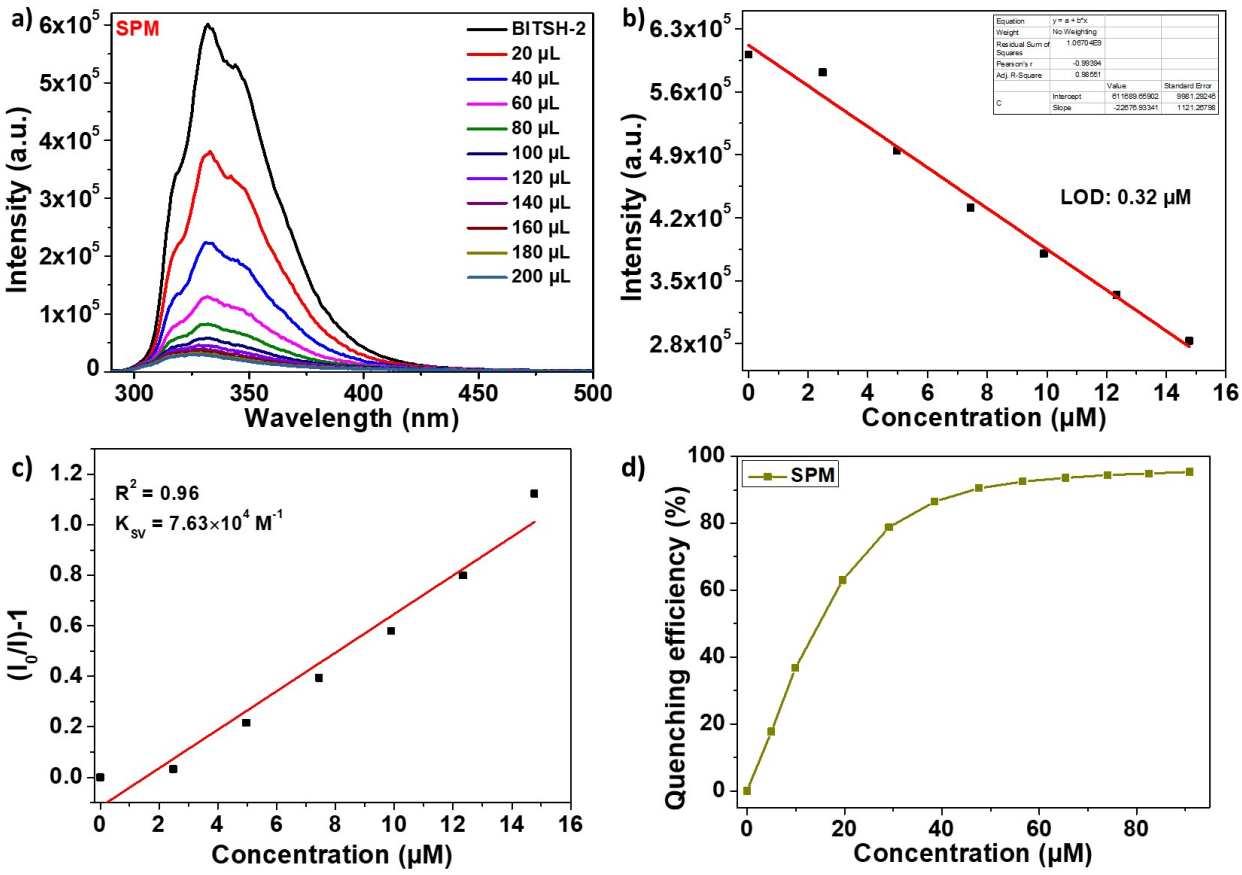

Figure S12. (a) PL emission spectra of BITSH-2 against the incremental additions of 1 mM of spermine (SPM) in ethanol, (λ_{ex} = 280 nm) **(b)** detection limit (LOD) of SPM, **(c)** linear fit of Stern-Volmer plot of BITSH-2 in response to SPM and **(d)** Quenching efficiency of SPM.

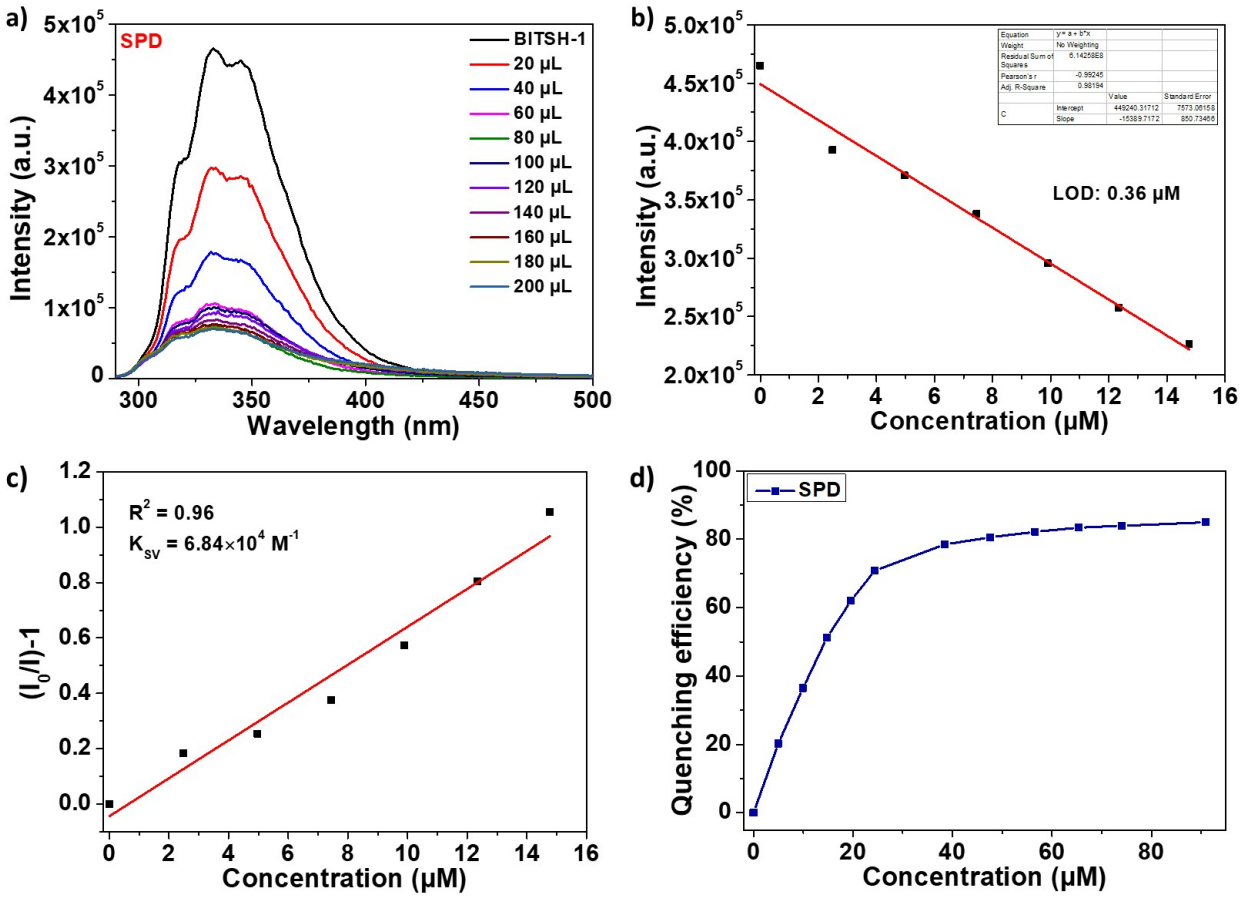

Figure S13. (a) PL emission spectra of BITSH-1 against the incremental additions of 1 mM of spermidine (SPD) in ethanol, (λ_{ex} = 278 nm) **(b)** detection limit (LOD) of SPD, **(c)** linear fit of Stern-Volmer plot of BITSH-1 in response to SPD and **(d)** Quenching efficiency of SPD.

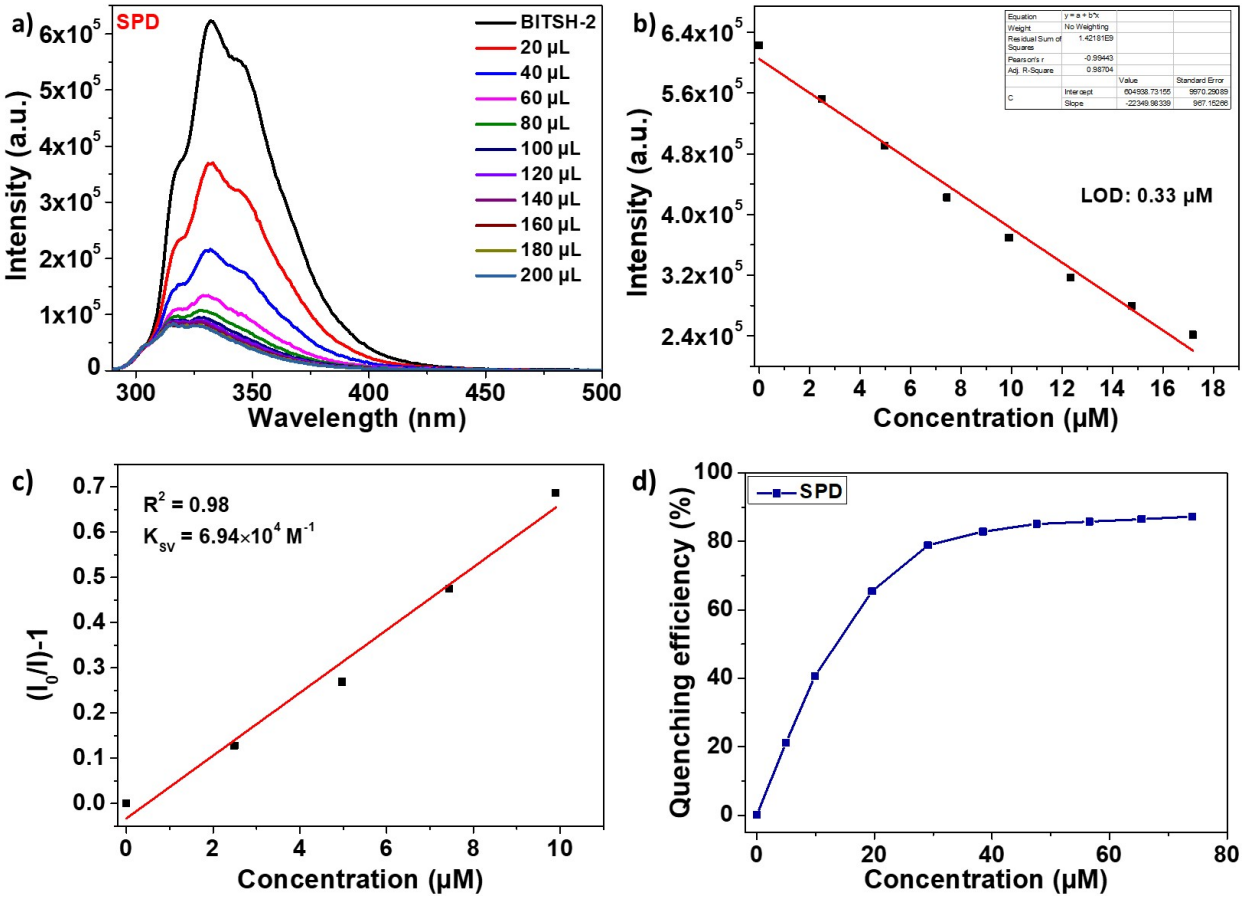

Figure S14. (a) PL emission spectra of BITSH-2 against the incremental additions of 1 mM of spermidine (SPD) in ethanol, (λ_{ex} = 280 nm) **(b)** detection limit (LOD) of SPD, **(c)** linear fit of Stern-Volmer plot of BITSH-2 in response to SPD and **(d)** Quenching efficiency of SPD.

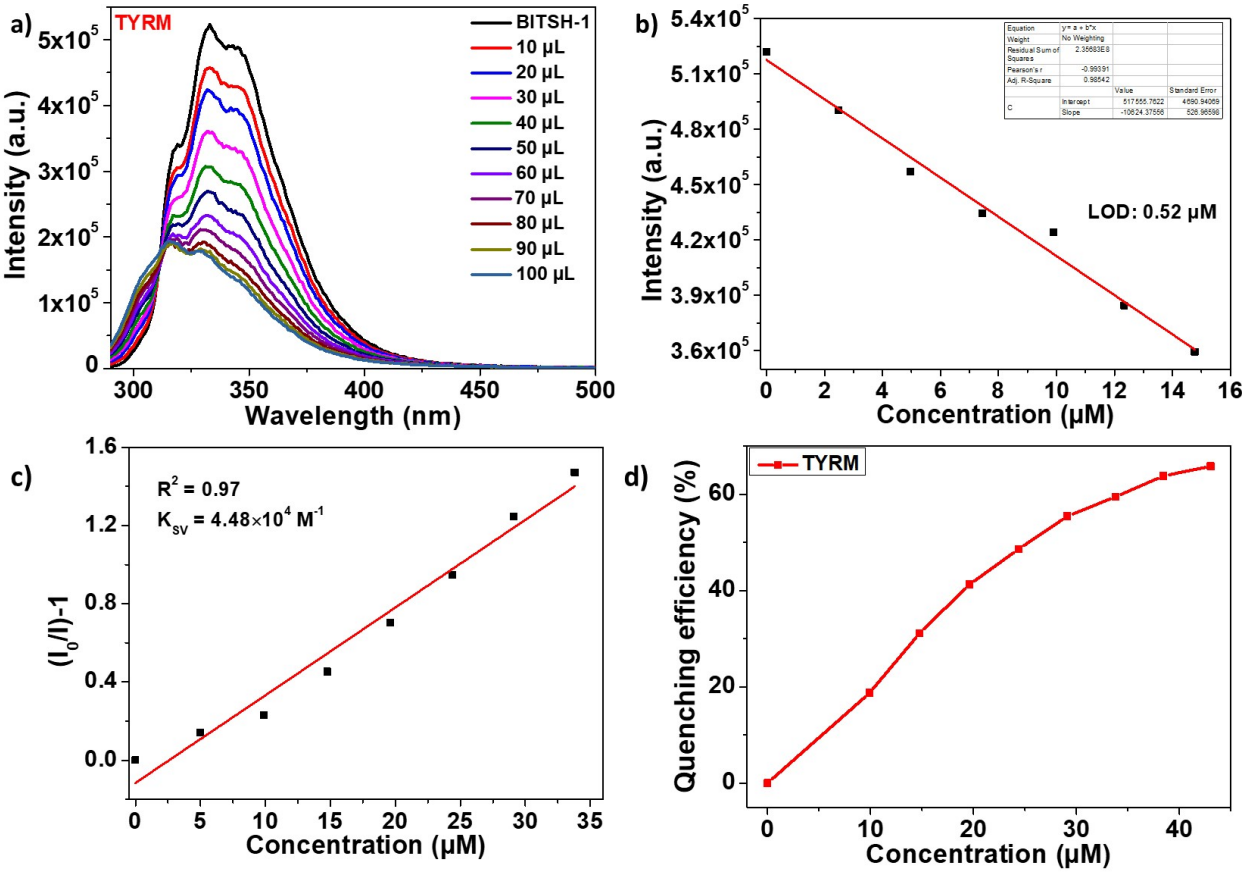

Figure S15. (a) PL emission spectra of BITSH-1 against the incremental additions of 1 mM of tyramine (TYRM) in ethanol, (λ_{ex} = 278 nm) **(b)** detection limit (LOD) of TYRM, **(c)** linear fit of Stern-Volmer plot of BITSH-1 in response to TYRM and **(d)** Quenching efficiency of TYRM.

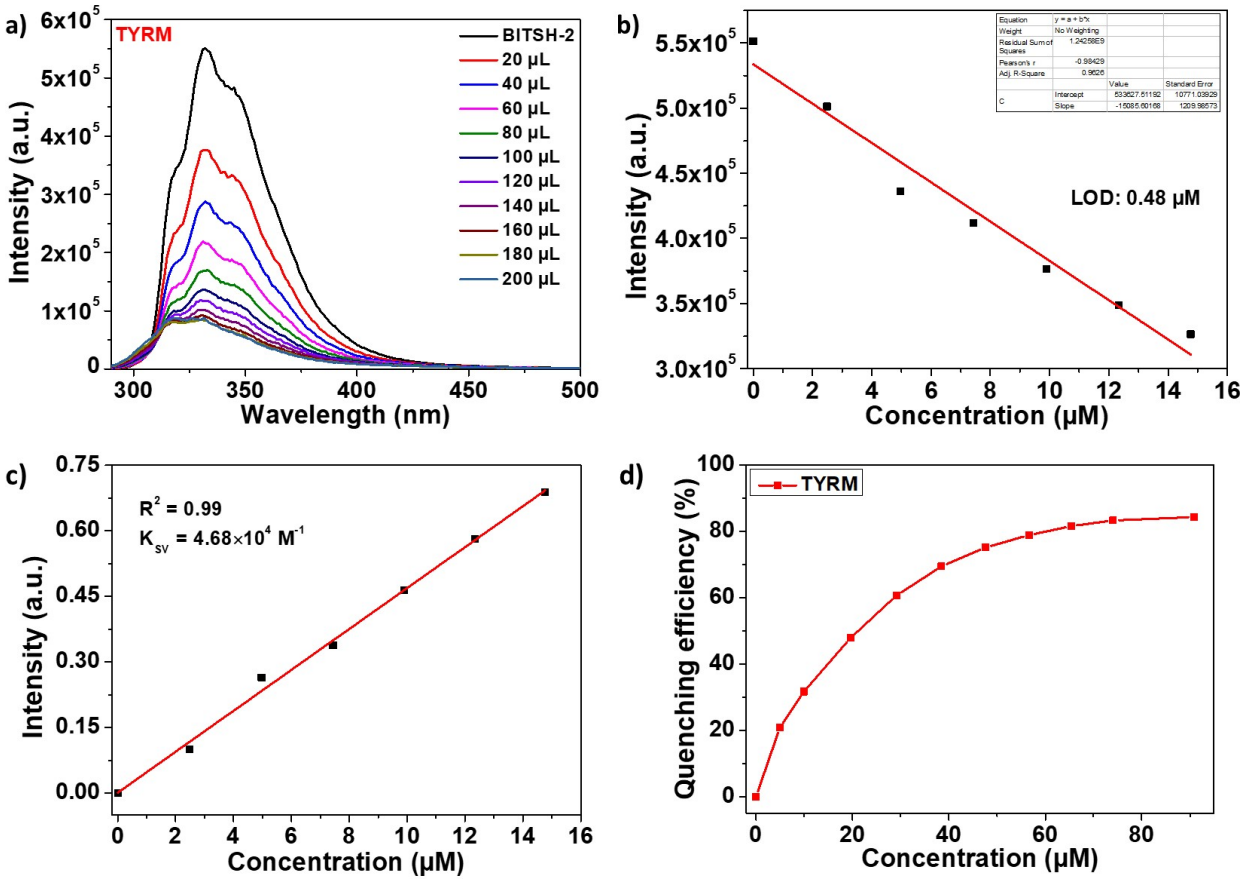

Figure S16. (a) PL emission spectra of BITSH-2 against the incremental additions of 1 mM of tyramine (TYRM) in ethanol, (λ_{ex} = 280 nm) **(b)** detection limit (LOD) of TYRM, **(c)** linear fit of Stern-Volmer plot of BITSH-2 in response to TYRM and **(d)** Quenching efficiency of TYRM.

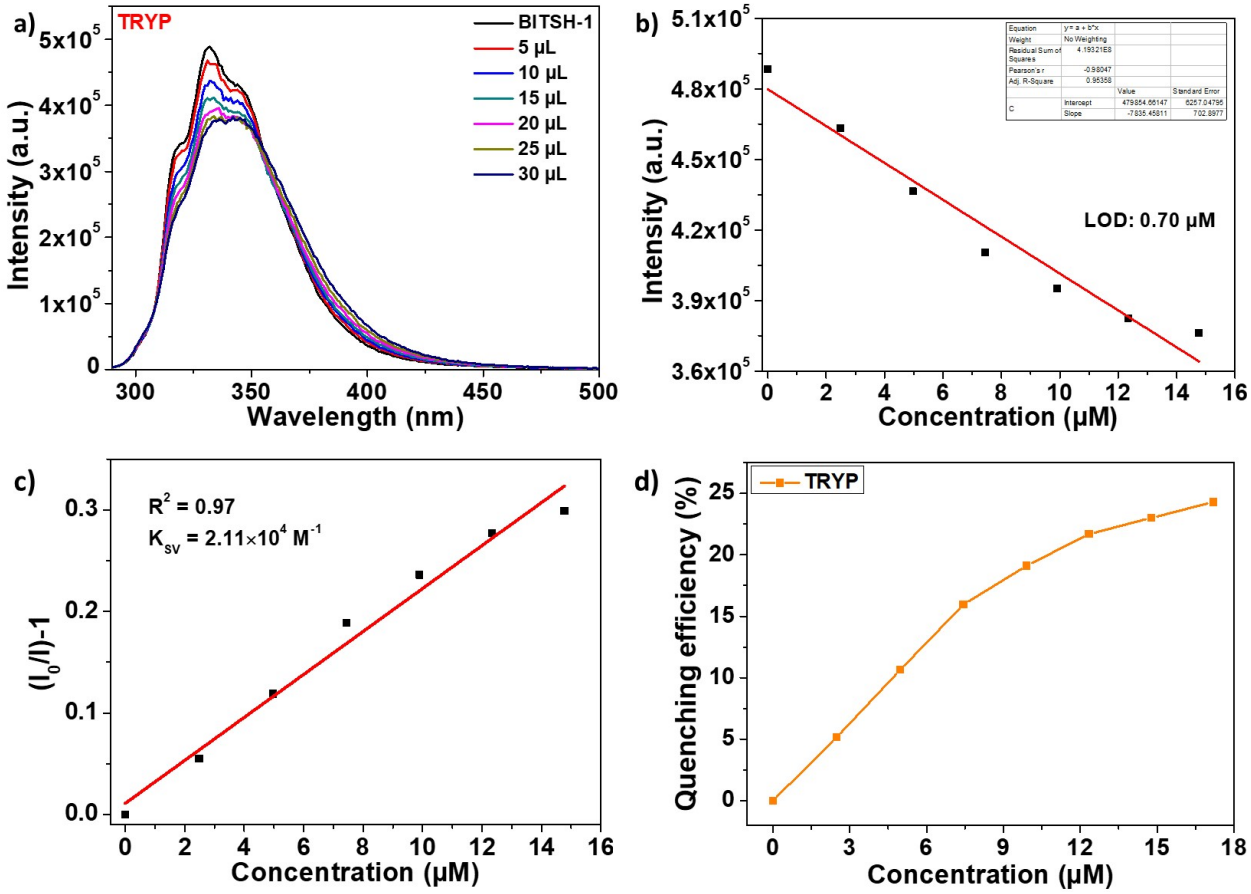

Figure S17. (a) PL emission spectra of BITSH-1 against the incremental additions of 1 mM of tryptamine (TRYP) in ethanol, (λ_{ex} = 278 nm) **(b)** detection limit (LOD) of TRYP, **(c)** linear fit of Stern-Volmer plot of BITSH-1 in response to TRYP and **(d)** Quenching efficiency of TRYP.

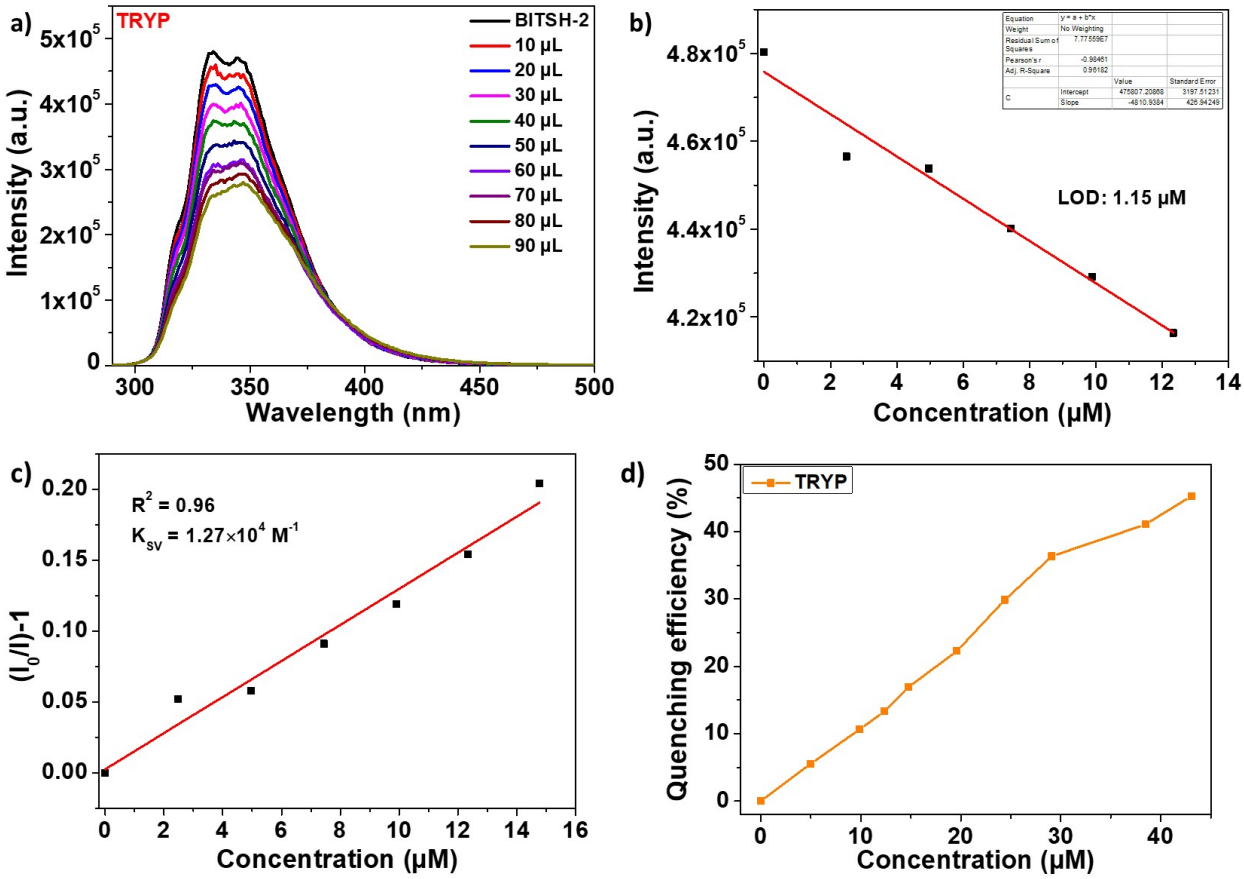

Figure S18. (a) PL emission spectra of BITSH-2 against the incremental additions of 1 mM of tryptamine (TRYP) in ethanol, (λ_{ex} = 280 nm) **(b)** detection limit (LOD) of TRYP, **(c)** linear fit of Stern-Volmer plot of BITSH-2 in response to TRYP and **(d)** Quenching efficiency of TRYP.

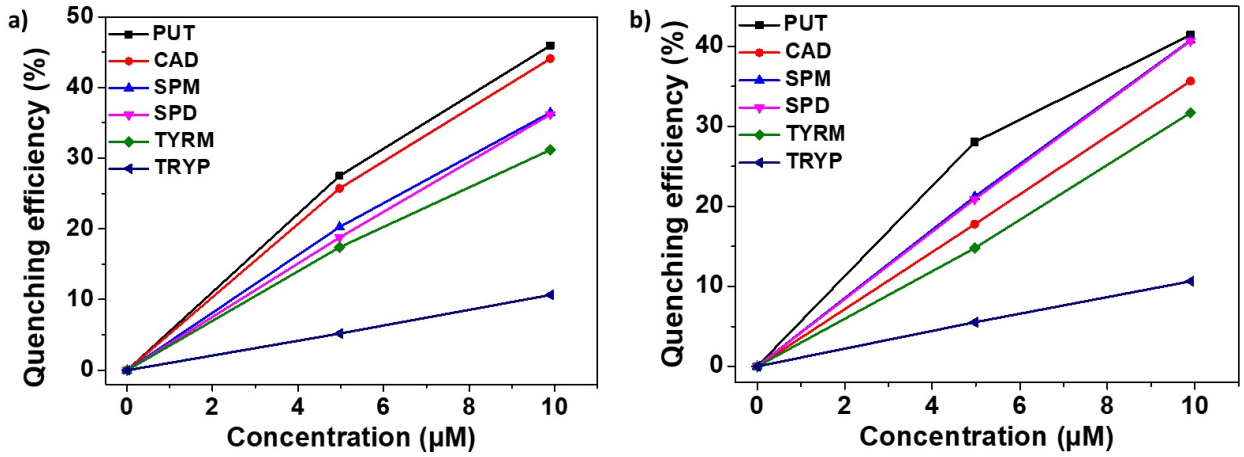

Figure S19. Quenching efficiencies of analytes in the concentration range of 0-10 μM on addition to (a) BITSH-1 and (b) BITSH-2.

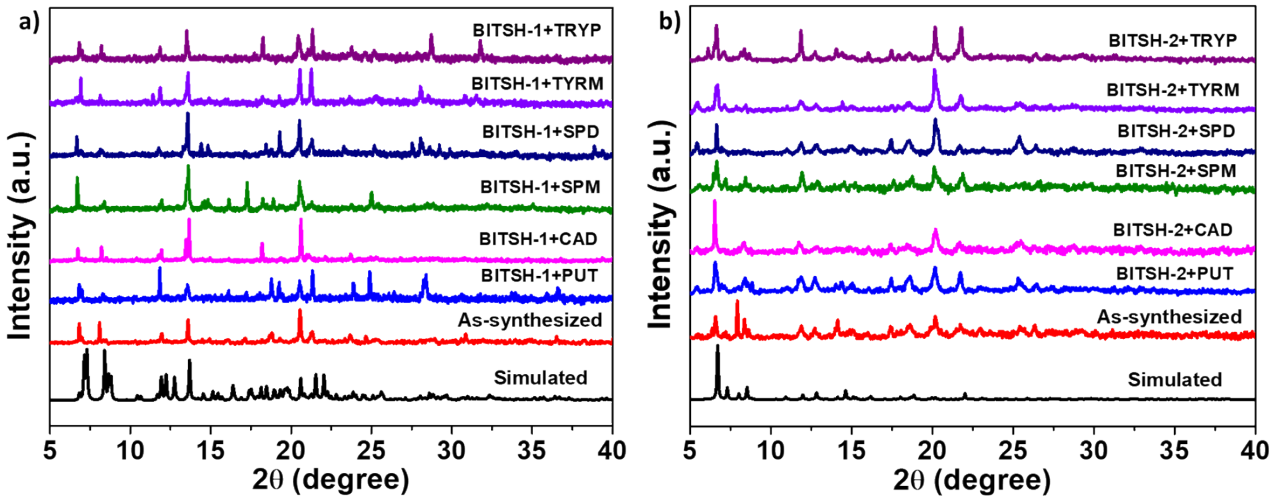

Figure S20. Comparison of the PXRD patterns of as-synthesized a) BITSH-1 and b) BITSH-2 in the presence of biogenic amines (BA).

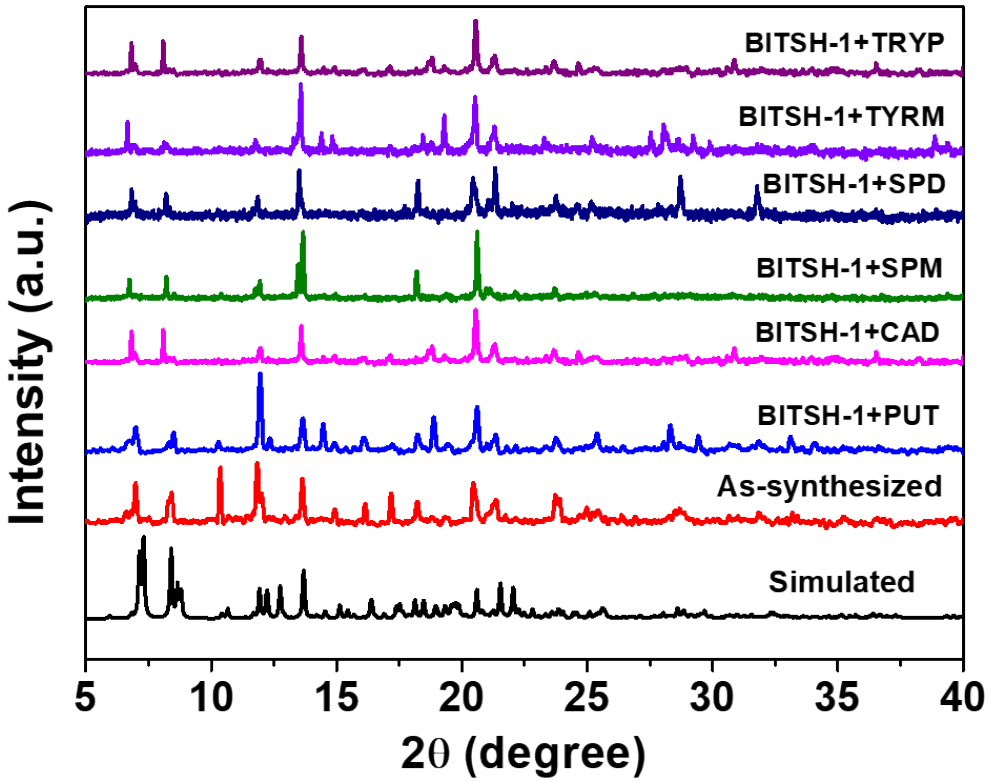

Figure S21. Comparison of the PXRD patterns of as-synthesized BITSH-1 in the presence of biogenic amines (BA), obtained by collecting the sample through centrifugation after fluorescence experiments and collected samples were dried at 100 °C.

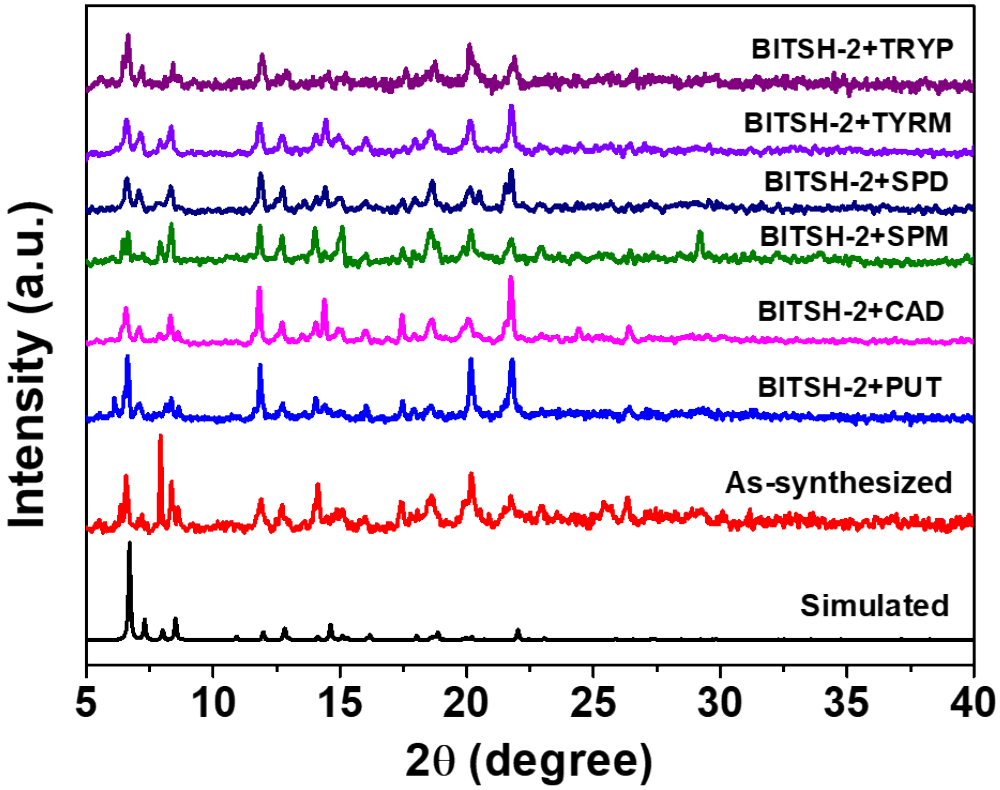

Figure S22. Comparison of the PXRD patterns of as-synthesized BITSH-2 in the presence of biogenic amines (BA), obtained by collecting the sample through centrifugation after fluorescence experiments and collected samples were dried at 100 °C.

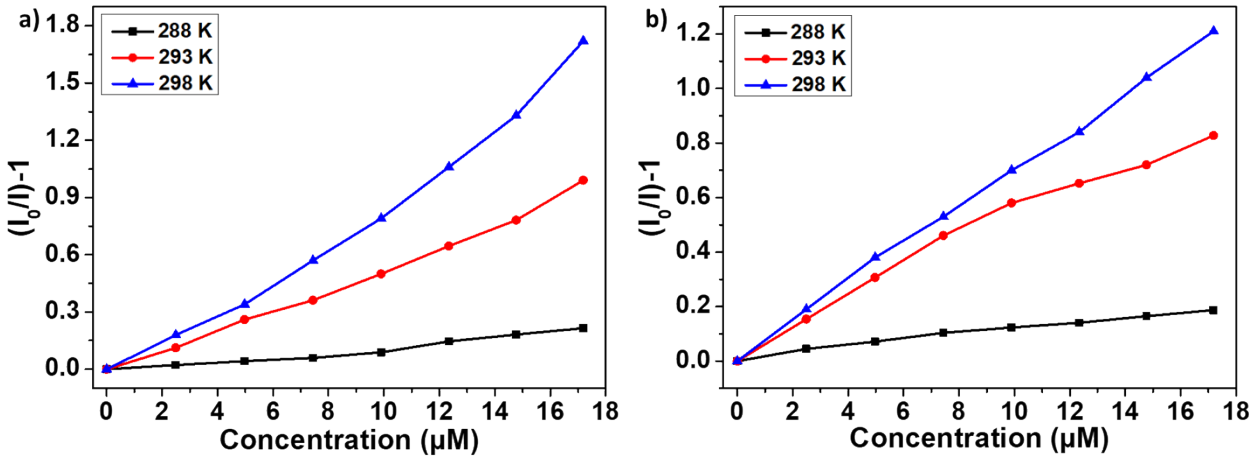

Figure S23. Stern Volmer plot of a) BITSH-1 and b) BITSH-2 on incremental additions of PUT (1 mM) recorded at different temperatures.

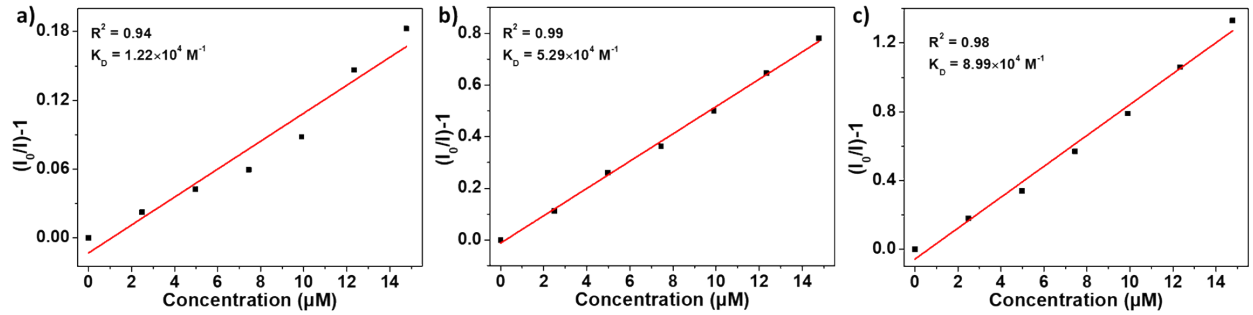

Figure S24. Linear fit of Stern-Volmer plot of BITSH-1 in response to PUT at different temperatures (a) 288 K (b) 293 K and (c) 298 K.

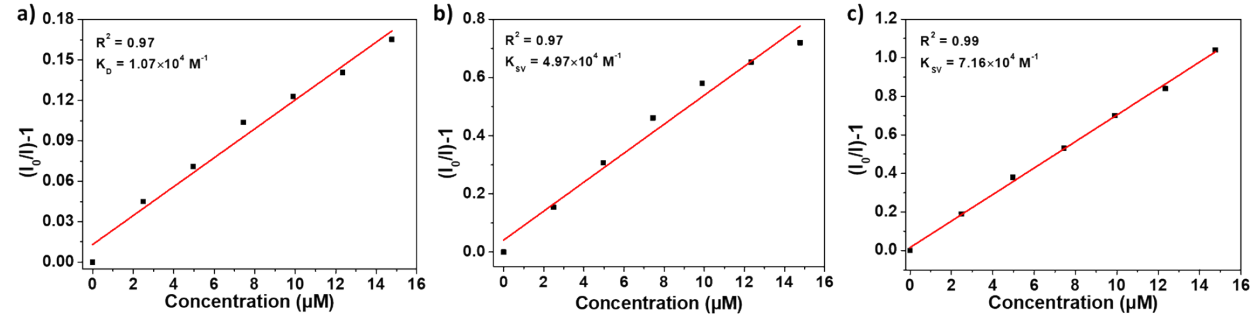

Figure S25. Linear fit of Stern-Volmer plot of BITSH-1 in response to PUT at different temperatures (a) 288 K (b) 293 K and (c) 298 K.

Table S2. K_D values of BITSH-1 and BITSH-2 obtained on incremental additions of PUT (1 mM) at different temperatures.

Temperature (K)	BITSH-1 K_D (M^{-1})	BITSH-2 K_D (M^{-1})
288 K	1.22×10^4	1.07×10^4
293 K	5.29×10^4	4.97×10^4
298 K	8.99×10^4	7.16×10^4

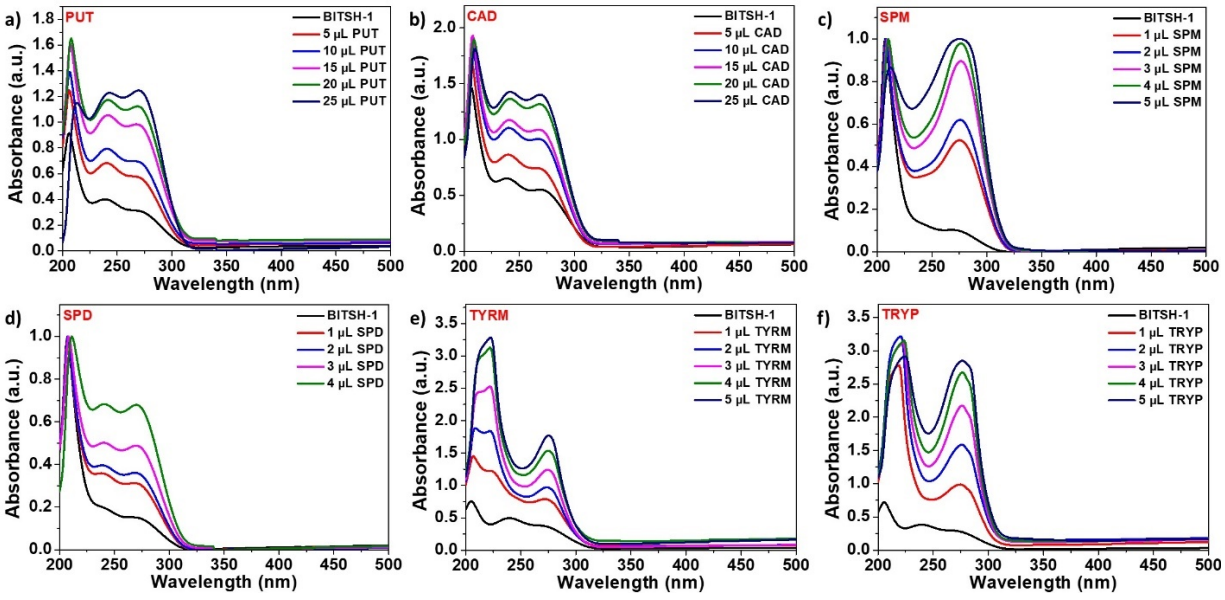

Figure S26. UV-vis spectra of BITSH-1 on addition of **(a)** PUT **(b)** CAD **(c)** SPM **(d)** SPD **(e)** TYRM **(f)** TRYP in ethanol medium.

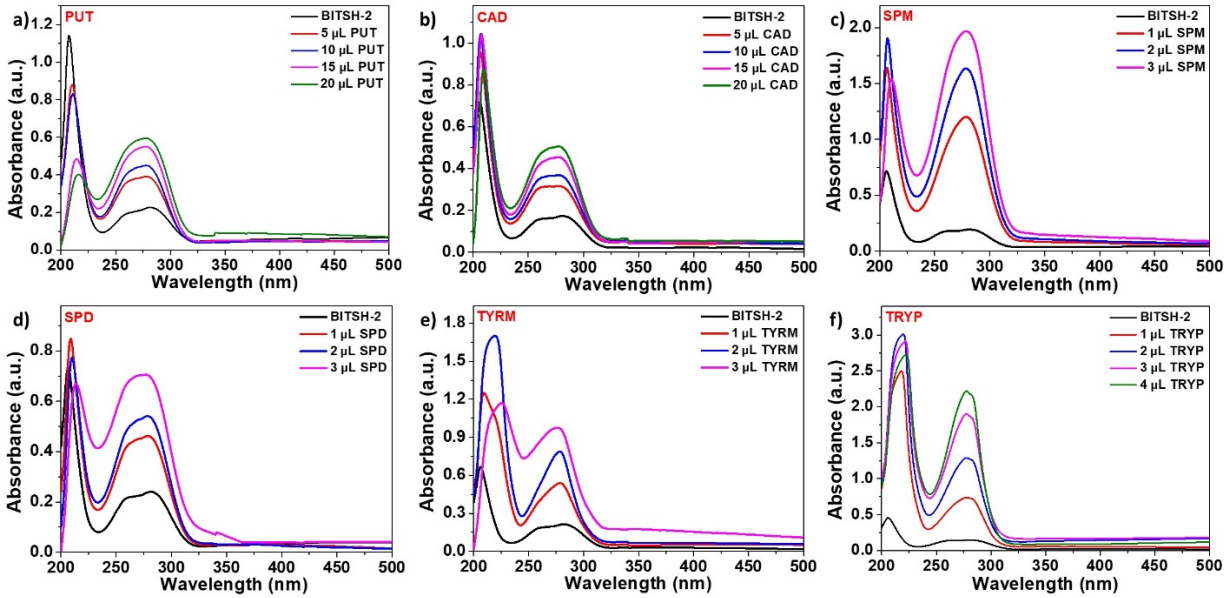

Figure S27. UV-vis spectra of BITSH-2 on addition of **(a)** PUT **(b)** CAD **(c)** SPM **(d)** SPD **(e)** TYRM **(f)** TRYP in ethanol medium.

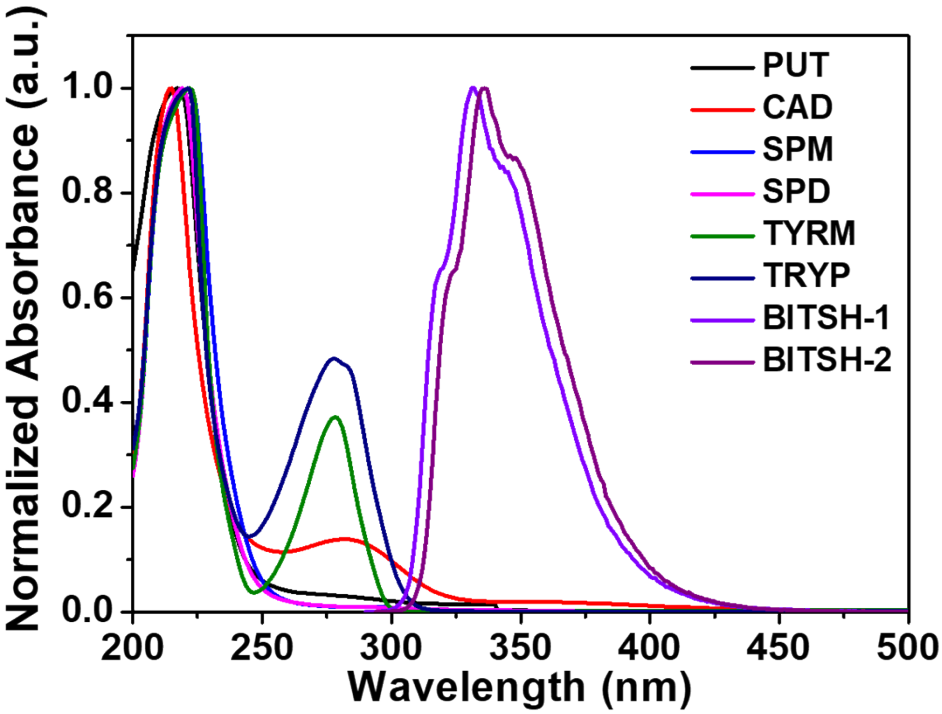

Figure S28. Spectral overlap between absorption spectra of analytes and emission spectra of both the MOF systems.

Electrochemical measurements

Electrochemical nature of BITSH-1 and BITSH-2 were studied using cyclic voltammetry with three electrode cell setup. The reduction and oxidation potentials were obtained at room temperature using Fluorine-doped Tin Oxide (FTO) as the working electrode, platinum mesh as counter electrode and Ag/AgCl as reference electrode. The measurements were carried out using 0.1 M tetrabutylammonium perchlorate in acetonitrile as electrolyte solution. The HOMO and LUMO energy levels were calculated considering the onset oxidation potential and reduction potential values obtained from the Cyclic Voltammogram (CV) and using the following equation.

$\mathbf{E_{HOMO} = -e\,[E_{ox\ onset} + 4.741]\ eV}$ and $\mathbf{E_{LUMO} = -e\,[E_{red\ onset} + 4.741]\ eV.}$[1]

The band gap of BITSH-1 and BITSH-2 was calculated using $\mathbf{E_g = LUMO - HOMO}$[1] and the band gap obtained was 2.7 eV for both the frameworks.

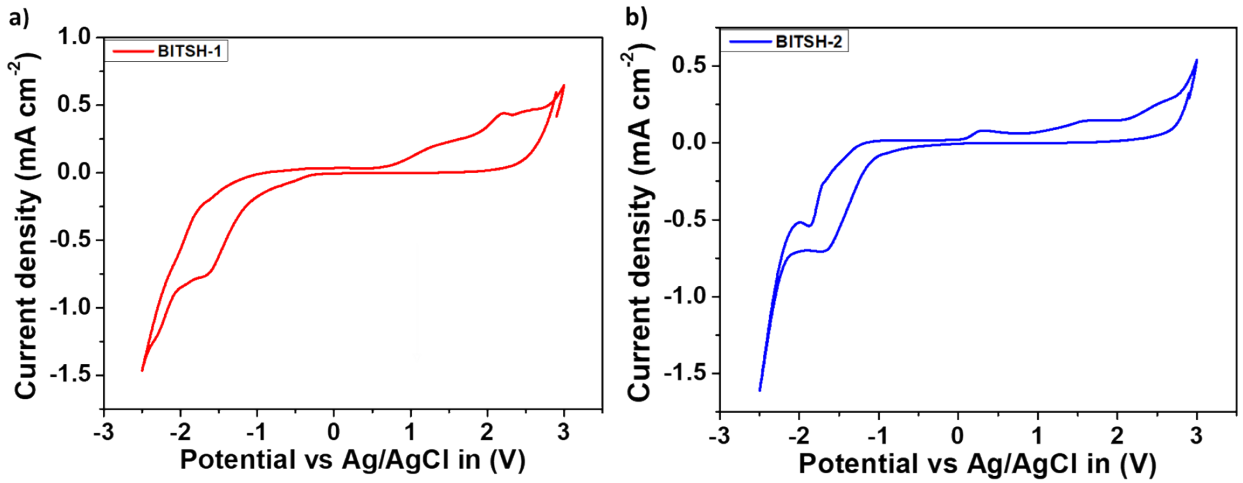

Figure S29. Cyclic Voltammogram (CV) of a) BITSH-1 and b) BITSH-2 recorded in acetonitrile medium.

X-ray Photoelectron Spectroscopy (XPS)

X-ray Photoelectron Spectroscopy (XPS) experiments were performed to identify the elemental composition, and the oxidation state of the elements present in both the MOF samples. X-ray Photoelectron Spectroscopy XPS was performed using Thermo Scientific, K- α instrument. The source used is Al K- α source [X-ray source 1486.8eV]. XPS analysis of both the frameworks were done and Fig. S8a,c shows the XPS survey spectra of BITSH-1 and BITSH-2 and the binding energies confirm the presence of Co, C, N and O elements. Fig. S8b,d depicts Co 2p XPS spectrum of both the frameworks and existence of Co as Co^{2+} with characteristic Co $2p_{1/2}$ at 781.5 eV and Co $2p_{3/2}$ peak at 797 eV. The binding energies of O1s, C1s and N1s were also obtained (Fig. S8-10).

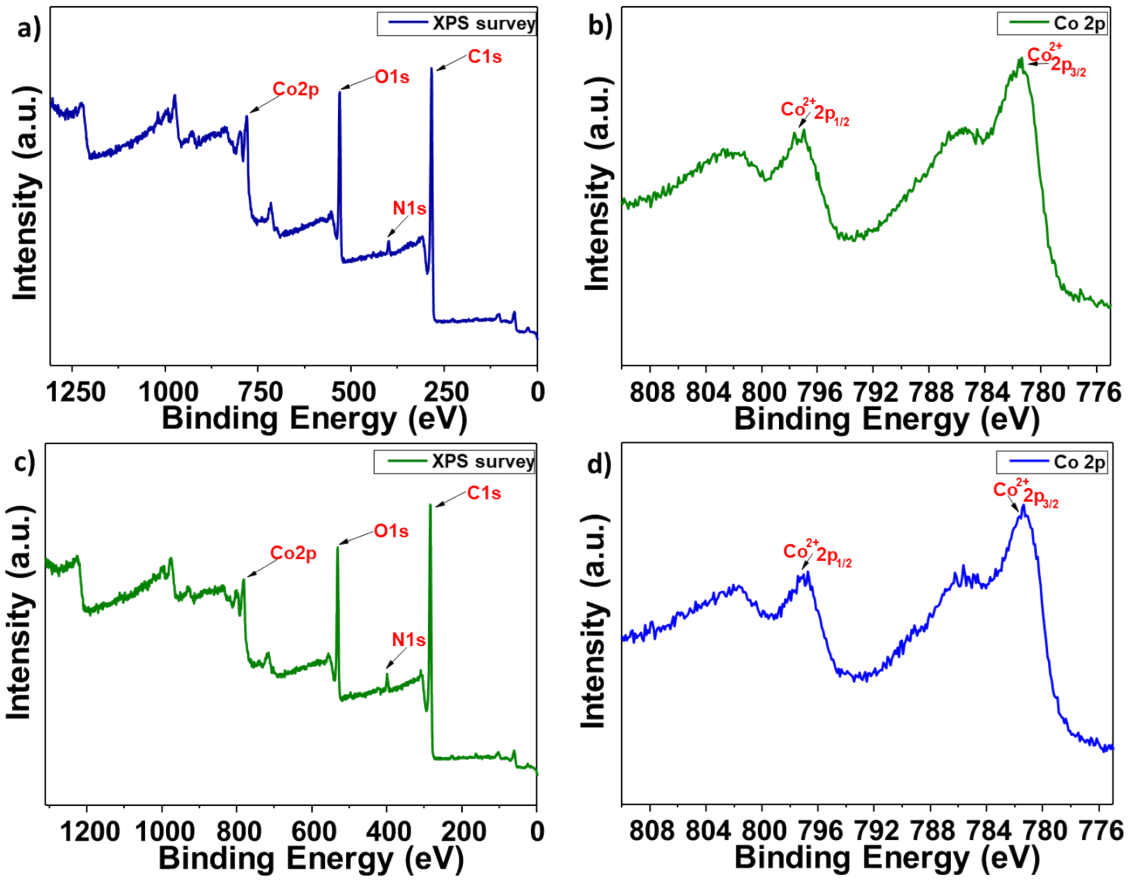

Fig. S30. XPS survey spectrum **(a)** and Co 2p XPS spectrum **(b)** of BITSH-1 sample, XPS survey spectrum **(c)** and Co 2p XPS spectrum **(d)** of BITSH-2 sample.

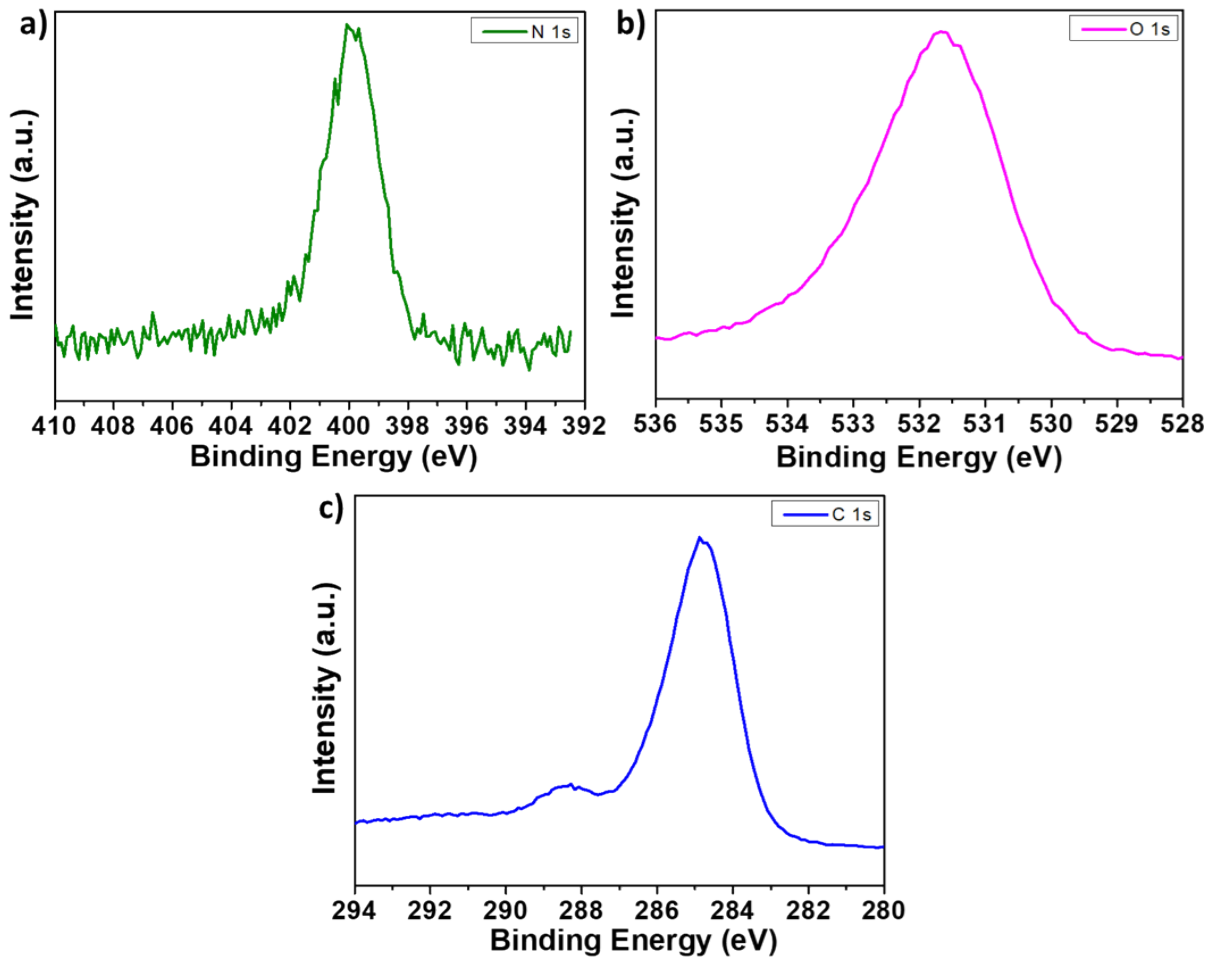

Figure S31. XPS spectra of BITSH-1 sample showing binding energies for a) N 1s, b) O 1s and c) C1s.

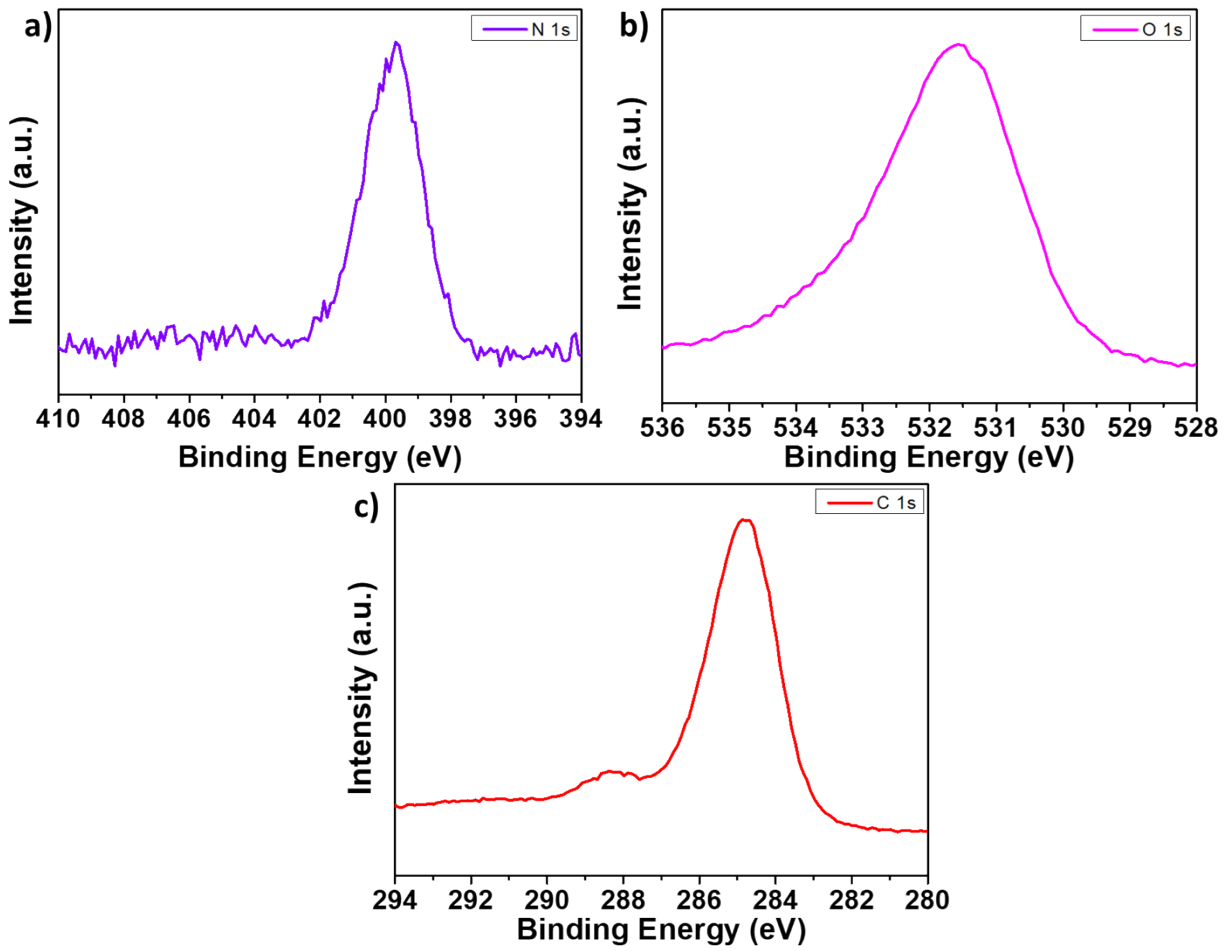

Figure S32. XPS spectra of BITSH-2 sample showing binding energies for a) N 1s, b) O 1s and c) C1s.

XPS analysis of MOF + Biogenic amines

The XPS analysis was carried out on both the MOFs before and after the fluorescence experiments in order to confirm the presence of biogenic amines such as PUT, CAD, SPM, SPD, TYRM and TRYP in the MOF systems. The N1s spectra of both the MOF systems were analysed for the characteristic amine peaks.

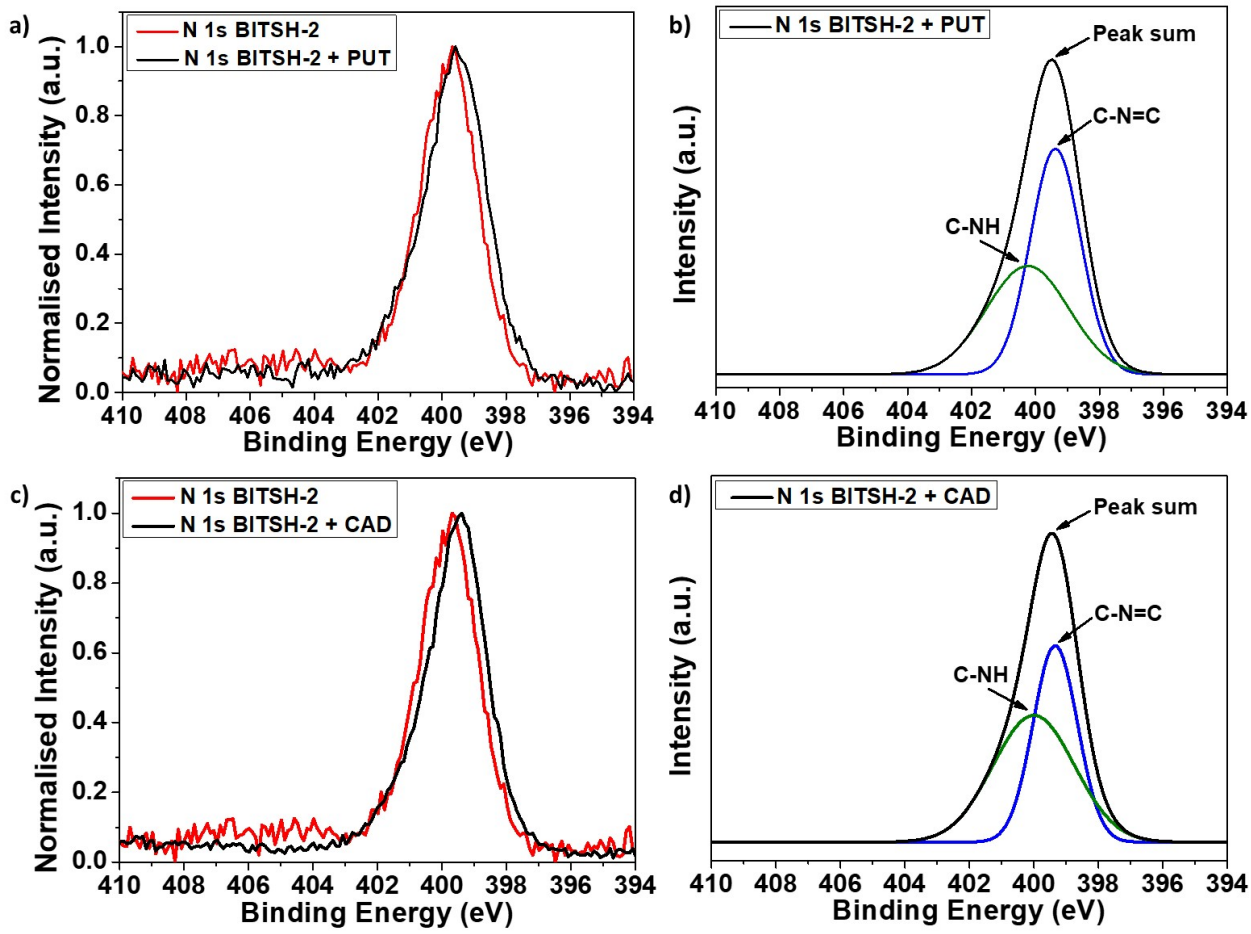

Figure S33. (a) N 1s XPS spectrum of BITSH-2 and on addition of PUT **(b)** Deconvoluted spectrum of BITSH-2 + PUT. **(c)** N 1s XPS spectrum of BITSH-2 and on addition of CAD **(d)** Deconvoluted spectrum of BITSH-2 + CAD.

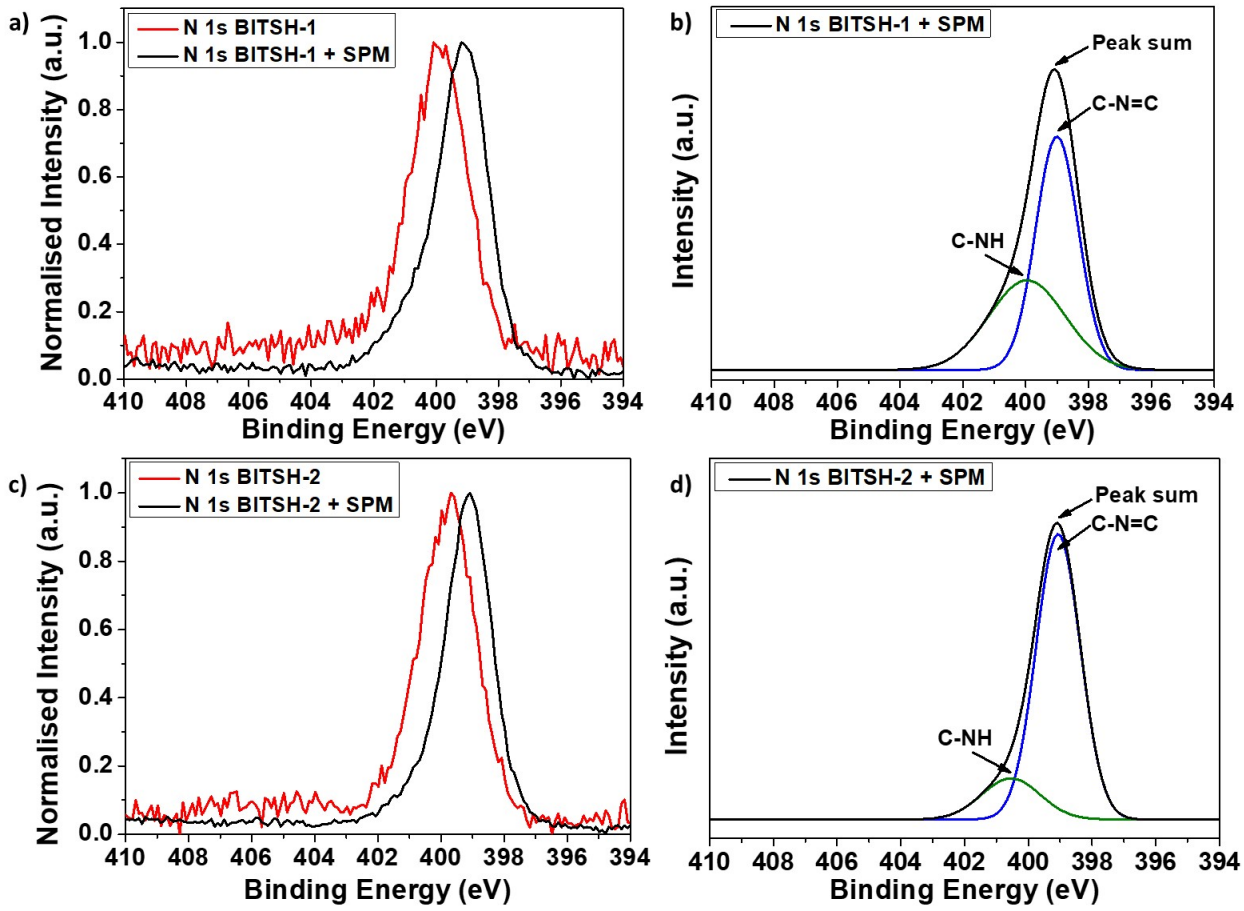

Figure S34. (a) N 1s XPS spectrum of BITSH-1 and on addition of SPM **(b)** Deconvoluted spectrum of BITSH-1 + SPM. **(c)** N 1s XPS spectrum of BITSH-2 and on addition of SPM **(d)** Deconvoluted spectrum of BITSH-2 + SPM.

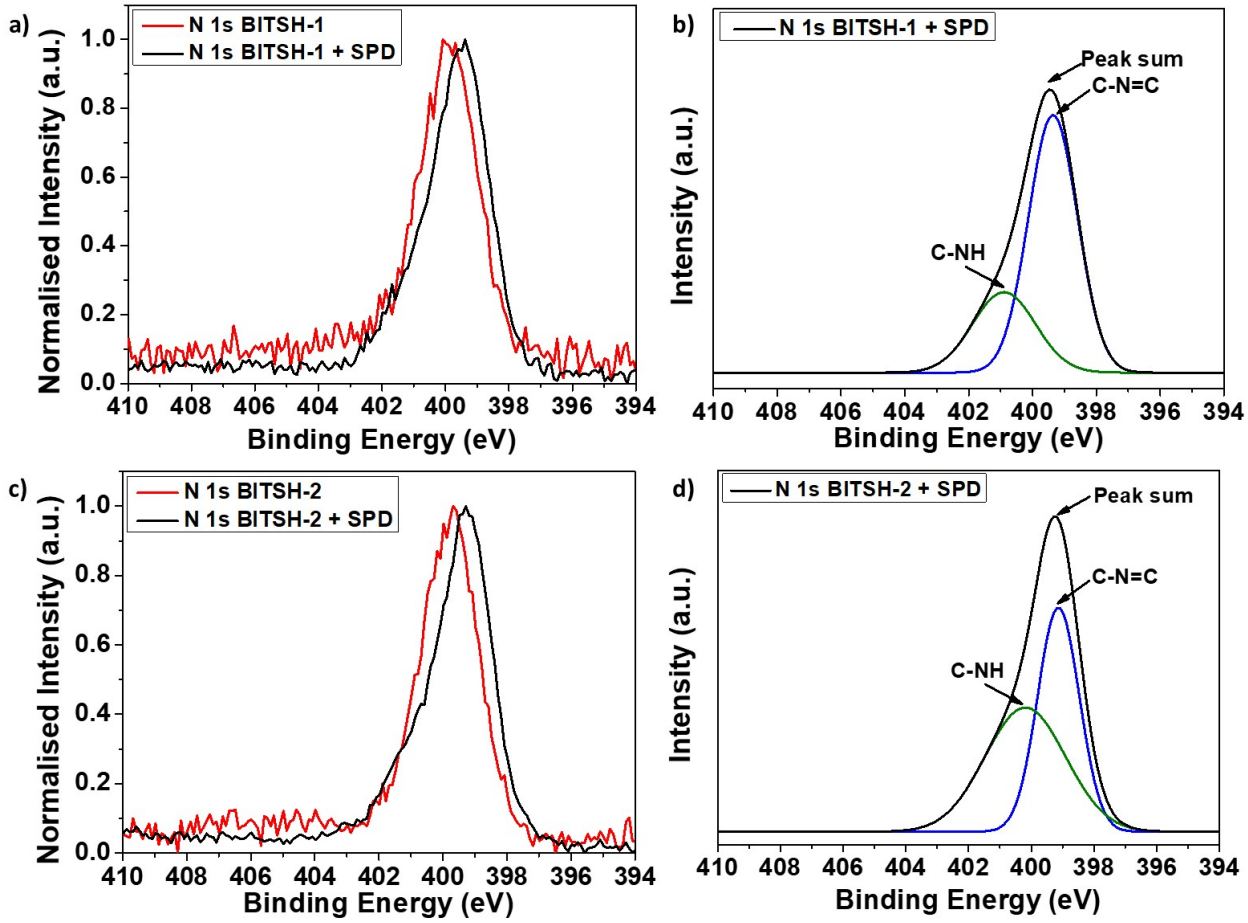

Figure S35. (a) N 1s XPS spectrum of BITSH-1 and on addition of SPD **(b)** Deconvoluted spectrum of BITSH-1 + SPD. **(c)** N 1s XPS spectrum of BITSH-2 and on addition of SPD **(d)** Deconvoluted spectrum of BITSH-2 + SPD.

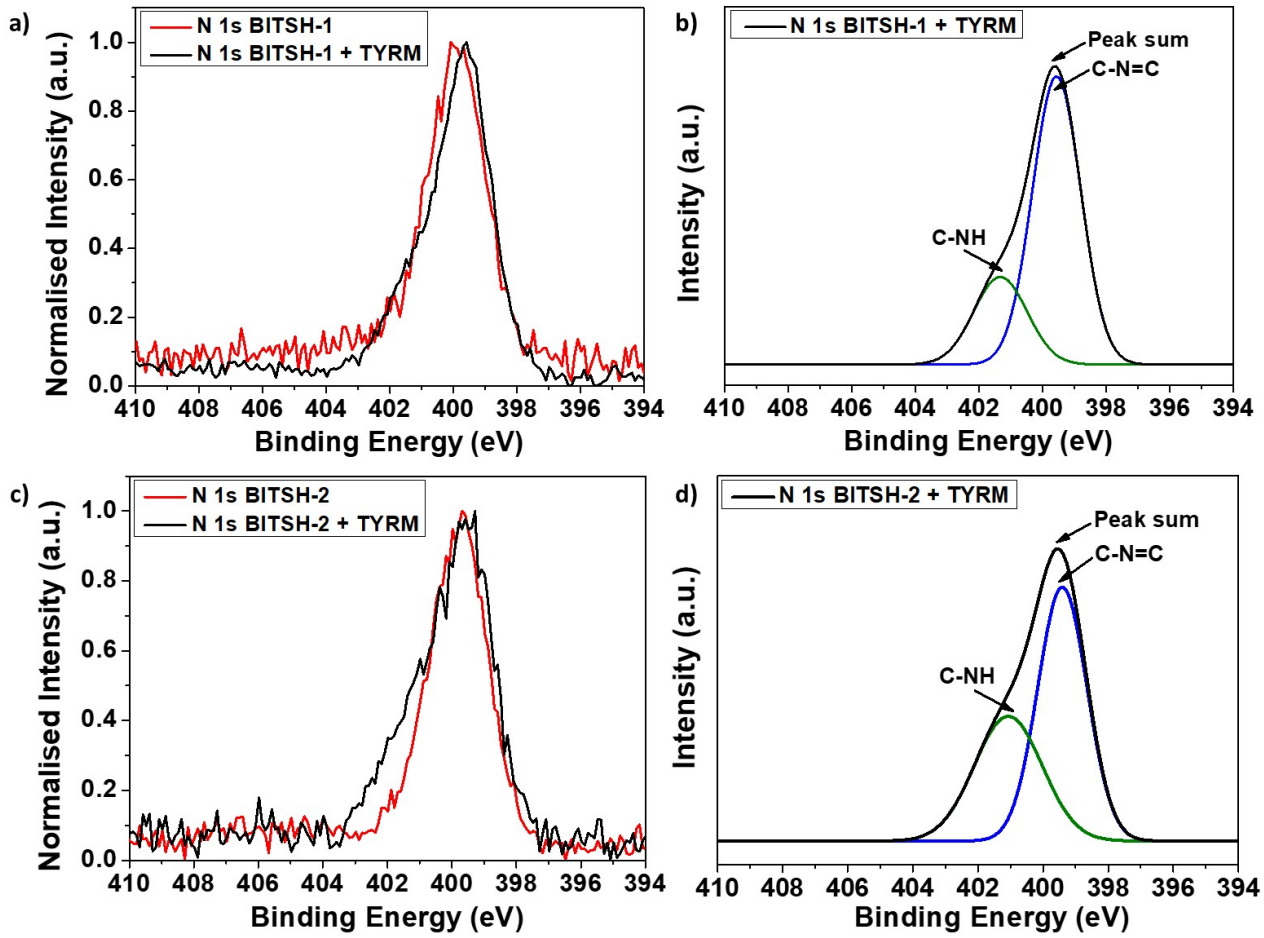

Figure S36. (a) N 1s XPS spectrum of BITSH-1 and on addition of TYRM **(b)** Deconvoluted spectrum of BITSH-1 + TYRM. **(c)** N 1s XPS spectrum of BITSH-2 and on addition of TYRM **(d)** Deconvoluted spectrum of BITSH-2 + TYRM.

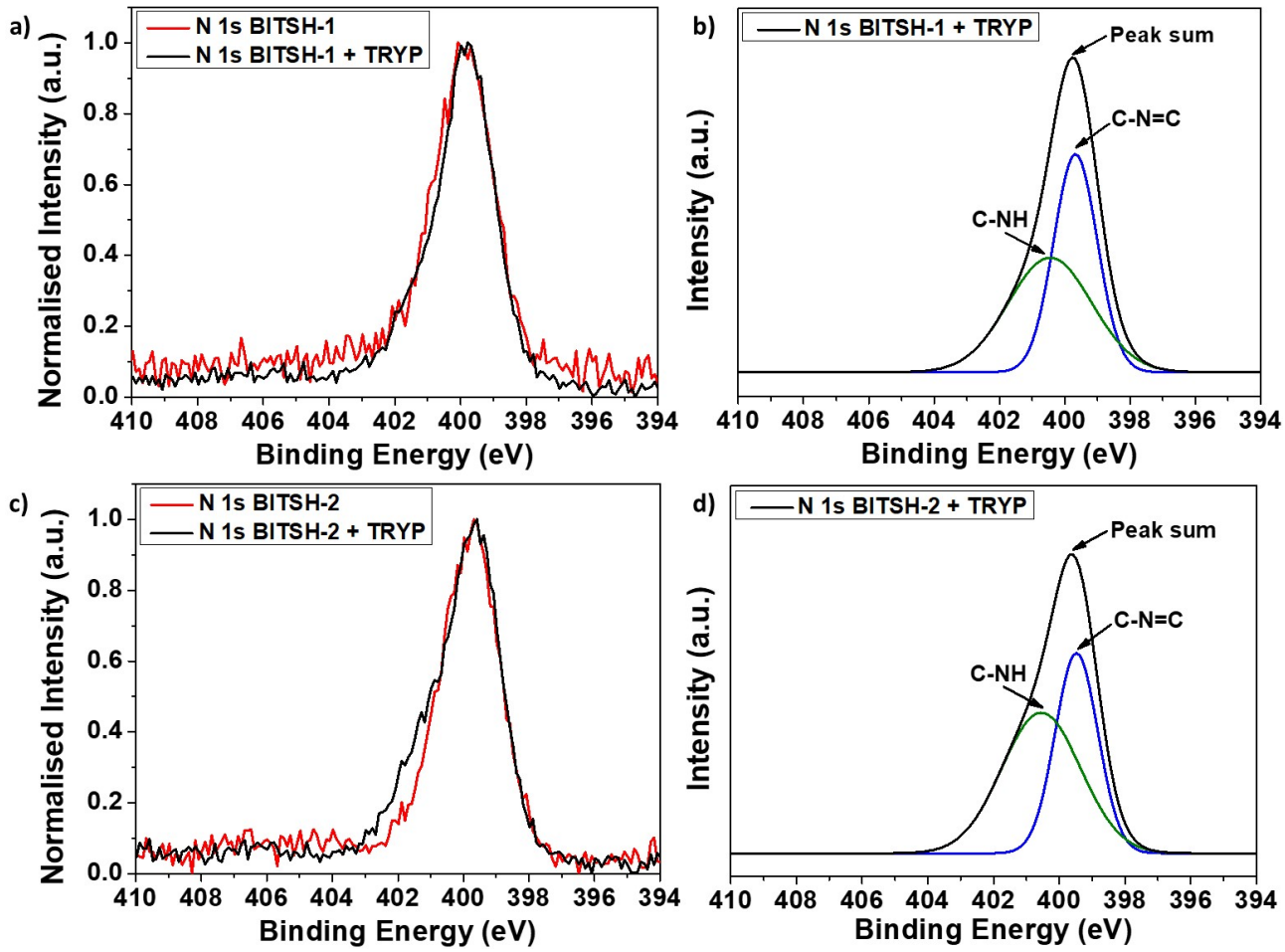

Figure S37. (a) N 1s XPS spectrum of BITSH-1 and on addition of TRYP **(b)** Deconvoluted spectrum of BITSH-1 + TRYP. **(c)** N 1s XPS spectrum of BITSH-2 and on addition of TRYP **(d)** Deconvoluted spectrum of BITSH-2 + TRYP.

Blank readings of BITSH-1 and BITSH-2

BLANK	MOF-1	MOF-2
Blank Reading 1	553885	473134
Blank Reading 1	553933	470702
Blank Reading 1	554002	472363
Blank Reading 1	551367	469254
Blank Reading 1	549985	467098
Standard deviation	1853.801	2427.711

Table S3. Comparison of different probes, techniques and detection limits for sensing biogenic amines

Biogenic amines	Sensor	Detection technique	Limit of Detection	Linear range	Reference
SPM, SPD	Anionic organic dye-Zincon	Colorimetric method	25.1 and 30.7 nM, respectively	0-5 μM	2
PUT-CAD-SPM-SPD-HIS	Zn(II) Schiff-base complex	Colorimetric method	2.2 μM PUT, 1.64 μM CAD, 0.97 μM SPM, 1.68 μM SPD, 1.02 μM HIS	0-18 μM	3
PUT-CAD-TYR-HIS	amino-reactive chameleon stain Py-1	Capillary electrophoresis	0.2 to 0.9 μM	1-100 μM	4
SPM, SPD	Complexes of Pb(II), Cd(II), and Zn(II)	Fluorescence turn-on	25 μM	25-250 μM	5
PUT-CAD-SPM-SPD-TYR-HIS	Dansyl chloride derivatization	HPLC	0.09 to 0.3 mg L^{-1},	NA	6
PUT, CAD	Trifluoroacetylacetone (TFAA) / On-fibre derivatisation	GC-MS	0.5–0.6 μg cm^{-3}	0-100 μg cm^{-3}	7
PUT, CAD	PSAO @ Nafion–MnO_2 in the SPCE	Electrochemical method	0.30 μM	1-50 μM	8
PUT, CAD	4-MBA-functionalized Au@ZIF-8 SERS paper	Surface-enhanced Raman scattering (SERS) technique	76.99 and 115.88 ppb, respectively	0-10^{-4} (v/v)	9
SPM	zwitterionic Cd-MOF	Fluorescence quenching	0.3 μM	NA	10
SPM	Pyrene derivative and squarine containing self-assembled system	Fluorescence quenching	4.73 μM	1-10 μM	11
PUT, CAD	Co-MOF	Fluorescence quenching	0.24 μM PUT, 0.28 μM CAD	0-16 μM	**This work**

PUT-putrescine, CAD-cadaverine, SPM-spermine, SPD-spermidine, TYR-tyramine, HIS-histamine, PSAO-pea seedling amino oxidase, MBA-mercatobenzaldehyde

References

1. L. Shi, C. He, D. Zhu, Q. He, Y. Li, Y. Chen, Y. Sun, Y. Fu, D. Wen, H. Cao and J. Cheng, *J. Mater. Chem.,* 2012, **22,** 11629-11635.
2. Y. Fukushima and S. Aikawa, *Tetrahedron Lett.,* 2019, **60,** 151302.
3. G. Munzi, S. Failla and S. Di Bella, *Analyst.*, 2021, **146**, 2144-2151.
4. M. S. Steiner, R. J. Meier, C. Spangler, A. Duerkop and O. S. Wolfbeis, *Microchim Acta.,* 2009, **167,** 259.
5. J. T. Fletcher and B. S. Bruck, *Sens. Actuators B.,* 2015, **207,** 843–848.

6. H. F. Kung, C. Y. Huang, C. M. Lin, L. H. Liaw, Y. C. Lee and Y. H. Tsai*, J. Food Drug Anal.,* 2015, **23,** 335–342.
7. M. Y. Khuhawar, A. A. Memon, P. D. Jaipal, M. I. Bhanger, *J Chromatogr B Biomed Sci Appl.,* 1999, **723,** 17-24.
8. D. Telsnig, K. Kalcher, A. Leitner and A. Ortner, *Electroanalysis.,* 2013, **25,** 47-50.
9. H. Kim, B. T. Trinh, K. H. Kim, J. Moon, H. Kang, K. Jo, R. Akter, J. Jeong, E. K. Lim, J. Jung, H. S. Choi, H. G. Park, O. S. Kwon, I. Yoon and T. Kang, *Biosens. Bioelectron.,* 2021, **179,** 113063.
10. S. Jindal, V. K. Maka and J. N. Moorthy, *J. Mater. Chem. C.,* 2020, **8,** 11449.
11. J. Tu, S. Sun and Y. Xu, *Chem. Commun.,* 2016, **52,** 1040-1043.